ONE STEP FLAME SPRAY PYROLYSIS OF NANOCRYSTALLINE AG DOPED TIO_2 FOR PHOTOCATALYTIC CO_2 REDUCTION

By

MISS Chamchuri BUMRUNGSINMON

A Thesis Submitted in Partial Fulfillment of the Requirements

for Master of Engineering (CHEMICAL ENGINEERING)

Department of CHEMICAL ENGINEERING

Graduate School, Silpakorn University

Academic Year 2020

การสังเคราะห์ผลึกนาโนไททาเนียเจือโลหะเงินในขั้นตอนเดียวโดยใช้เทคนิคเฟลมสเปรย์ไพโรไลซิสสำหรับปฏิกริยารีดักชันของแก๊สคาร์บอนไดออกไซด์โดยใช้การเร่งปฏิกริยาด้วยแสง

โดย
นางสาวจามจุรี บำรุงสินมั่น

วิทยานิพนธ์นี้เป็นส่วนหนึ่งของการศึกษาตามหลักสูตรวิศวกรรมศาสตรมหาบัณฑิต
สาขาวิชาวิศวกรรมเคมี แผน ก แบบ ก 2 ระดับปริญญามหาบัณฑิต
ภาควิชาวิศวกรรมเคมี
บัณฑิตวิทยาลัย มหาวิทยาลัยศิลปากร
ปีการศึกษา 2563

ONE STEP FLAME SPRAY PYROLYSIS OF NANOCRYSTALLINE AG DOPED TIO_2 FOR PHOTOCATALYTIC CO_2 REDUCTION

By

MISS Chamchuri BUMRUNGSINMON

A Thesis Submitted in Partial Fulfillment of the Requirements

for Master of Engineering (CHEMICAL ENGINEERING)

Department of CHEMICAL ENGINEERING

Graduate School, Silpakorn University

Academic Year 2020

Title	ONE STEP FLAME SPRAY PYROLYSIS OF NANOCRYSTALLINE Ag DOPED TiO_2 FOR PHOTOCATALYTIC CO_2 REDUCTION
By	Chamchuri BUMRUNGSINMON
Field of Study	(CHEMICAL ENGINEERING)
Advisor	Okorn Mekasuwandumrong

Graduate School Silpakorn University in Partial Fulfillment of the Requirements for the Master of Engineering

.....Dean of graduate school

(Associate Professor Jurairat Nunthanid, Ph.D.)

Approved by

.....Chair person

(Worapon Kiatkittipong)

.....Advisor

(Okorn Mekasuwandumrong)

.....Committee

(JOONGAI PANPRANOT)

.....Committee

(NUTCHAPON CHOTIGKRAI)

620920029 : Major (CHEMICAL ENGINEERING)
Keyword : CO2 reduction, Ag/TiO2, Methane, Flame Spray Pyrolysis (FSP), Photocatalyst

MISS CHAMCHURI BUMRUNGSINMON : ONE STEP FLAME SPRAY PYROLYSIS OF NANOCRYSTALLINE AG DOPED TIO_2 FOR PHOTOCATALYTIC CO_2 REDUCTION THESIS ADVISOR : OKORN MEKASUWANDUMRONG

In this research, nanocrystalline silver (Ag) deposited on TiO_2 support (Ag/TiO_2) photocatalysts were prepared by dry impregnation method (IM) using commercial TiO_2 (P25) as a support and flame spray pyrolysis (FSP) using titanium (IV) isopropoxide and silver nitrate as a Ti and Ag sources, respectively. The physiochemical properties of all photocatalyst were characterized by several techniques such as X-ray diffraction (XRD), UV-Vis spectroscopy, Photoluminescence spectrometer (PL), Transmission electron microscopy (TEM), X-ray photoelectron spectroscopy (XPS) and N_2-physicsorption (BET). The activities of photocatalyst were studied in photocatalytic CO_2 reduction under UV irradiation at room temperature. The TEM result of IM-made catalyst exhibited a regular shape and well-dispersed Ag particles with the particle size around 2-3 nm. This result is similar to FSP-made catalyst. The XRD pattern of FSP-7%wt Ag/TiO_2 photocatalyst showed the peak positions of silver metal phase while, the peak of Ag metal of other FSP-Ag/TiO_2 and IM-Ag/TiO_2 were not observed. This could be due to the fine dispersion of Ag metal on those supports or formation of amorphous particles. Increasing of Ag doping contents on TiO_2 leaded to the decrease of the PL spectra. The band gap energy (E_g) was also decreased as the Ag loading content increased. The FSP-Ag/TiO_2 displayed the yield of methane (umol/gCat.h) higher than pure TiO_2 and the IM-Ag/TiO_2. The energy band gap of all Ag/TiO_2 was decreased by increasing Ag doped on TiO_2. All Ag/TiO_2 photocatalysts exhibits the photoactivity higher than pure TiO_2. The best activity is FSP-7%wt Ag/TiO_2 photocatalyst. The effect of the enhanced adsorption UV light, less recombination rate and less energy bandgap cause the highest photocatalytic activity.

มหาวิทยาลัยศิลปากร

ACKNOWLEDGEMENTS

The author is really grateful for Associate Professor Okorn Mekasuwandumrong. He is support, guidance and inspiration in this thesis. Moreover, I would like to thank a chairman and the committees for your correctness and suggestion.

Furthermore, I am grateful to thank the Research and Development Institute of Silpakorn University for supporting the equipment and laboratory, the National metal and Materials Technology Center (MTEC) for Transmission electron microscopy (TEM), Center of Excellence on Catalysis and Catalytic reaction Engineering of Chulalongkorn University for X-ray diffraction (XRD), UV-Vis spectroscopy, Photoluminescence spectrometer (PL) and X-ray photoelectron spectroscopy (XPS).

Chamchuri BUMRUNGSINMON

TABLE OF CONTENTS

LIST OF TABLES

Page

LIST OF FIGURES

Page

CHAPTER I

INTRODUCTION

1.1 Motivation

Global warming and climate change have become one of the biggest hazards on the earth due to many causes on all living things on the planet. The primary source of greenhouse gases is carbon dioxide (CO_2) in the atmosphere. An increase in nearly 8 ppm of CO_2 has been reported for the period of 2011 to 2014 and it reached 398.55ppm in 2014 [1]. Presently, carbon dioxide (CO_2) concentration is increased because of the burning from the consumption of waste, human activities, industrial factory and fossil fuel such as coal power plant, oil and natural gas [7-9]. The growing consumption of these reason hazardous environmental pollutions [10-13]. The conversion of carbon dioxide (CO_2) into fuels such as carbon monoxide (CO), methane (CH_4), methanol (CH_3OH), formic acid (HCOOH), formaldehyde (HCHO) [14] and hydrogen (H_2) has become one of most inventing technologies to reduce global warming and the energy crisis [15-17]. The technology to convert CO_2 into worthwhile chemicals is the best choice because it is greener and low cost [1].

Therefore, a matter of great concern and any try to reduce CO_2 emission is importance [2]. There are three reaction types to convert CO_2 to other valuable products including: Thermal-catalysis, Electro-catalysis and Photo-catalysis [18]. Photo-catalysis was interested because of the increasing non-renewable fossil fuel energy sources. These are coal and natural gas that can be exhausted by the utilizations of light. The reaction is activated by exposure to near UV irradiation under mind ambient condition because the earth has abundant average solar irradiation [19]. In a photocatalytic process when a photocatalyst is exposed to light with sufficient energy, electron and hole are generated in the conduction and valence bands, respectively [20]. Following their migration to the surface of the photocatalyst, redox reactions between the adsorbed species on the surface and the photogenerated charge carriers occur [21]. Therefore, the separation between electron-hole pairs becomes crucial because the recombination of electron and hole has a negative effect on the performance of the photocatalyst.

In this report, photocatalysis reaction is used to solve this problem because economical, affordable and environmentally sustainable source of renewable energy. Titanium dioxide (TiO_2) was selected because it is the most suitable catalyst for this environmental application due to its nontoxicity, biological and chemical inertness [5], resistant oxidization and the stability in preparation for corrosion [19, 22-25]. Consequently, an important activity is the revelation and improvement of photocatalytic activity for feasible applications [26-28]. Recently, the attention of scientist has been attracted by the effect of metal doping [5, 29-32]. The metal doping is Silver (Ag) because it is high stability, great electrical and thermal conductivity appears a favorable doped on TiO_2 [5].

1.2 Objective of Research

Study the effect of silver (Ag) loading and catalyst preparation method on the physicochemical and photocatalytic properties of Ag/TiO_2 photocatalyst in photocatalytic CO_2 reduction.

1.3 Scope of Research

1.3.1 Prepare pure TiO_2 and silver (Ag) loading on TiO_2 catalysts by using Flame spray pyrolysis methods and dry impregnation. The proportion of silver (Ag) loading on TiO_2 was varied from 1, 3, 5 and 7 wt.%.

1.3.2 The catalyst was characterized by

1.3.3.1 N2-physicsorption (BET)

1.3.3.2 UV-Vis Spectrophotometer

1.3.3.3 X-ray diffractometer (XRD)

1.3.3.4 Photoluminescence spectrometer (PL)

1.3.3.5 Transmission electron microscopy (TEM)

1.3.3.6 X-ray photoelectron spectroscopy (XPS)

1.3.3 The obtain catalyst was tested in the photocatalytic reduction of CO_2 under UV radiation and the pH of reaction solution was varied adding different concentration of sodium hydroxide (NaOH).

1.3.4 Reaction gases were analyzed by using chromatography (GC-14B and GC-8A, Shimadzu).

1.4 Contribution of Research

This research presents the interested strategy for decreased amount of CO_2 in atmosphere that is the main cause of global warming. Silver (Ag) loading on TiO_2 catalysts were improved the CO_2 photocatalytic reduction activity and selectivity of hydrocarbon (C_xH_y).

CHAPTER II

LITERATURE REVIEWS

In this research, we interested on the CO_2 photocatalytic reduction of silver (Ag) loading on TiO_2 photocatalyst. The literature reviews discuss about the effect of silver (Ag) loading on physicochemical and photocatalytic properties of Ag/TiO_2 photocatalyst.

2.1 Photocatalytic of CO_2 reduction over TiO_2

Li et al. [6] studied the synthesis and characterization of Cu_2O/TiO_2 photocatalysts for H_2 evolution from aqueous solution with different scavengers. They synthesized the Cu_2O/TiO_2 photocatalysts by an ethanol reduction method using P25 as a support. The photocatalytic reaction was tested under 1 atm at 40ºC in 500mL closed quartz reactor system with UV irradiation. There are 3 aqueous solutions (ethylene glycol, methanol, anhydrous ethanol and glycerol) and it was added 450mL/batch. The 2.5mol%Cu_2O/TiO_2 exhibited the optimal photocatalytic activity which is better than pure P25. The amount of Hydrogen (H_2) is 2,048.25μmol/g.h in 10vol%methanol solution.

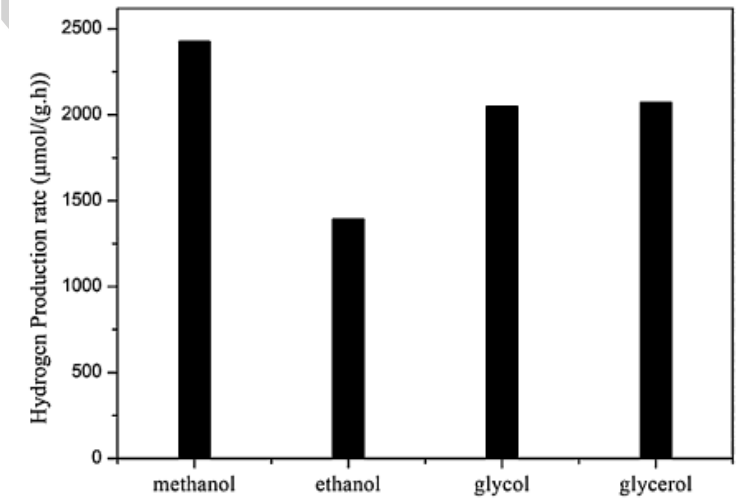

Figure 1: Photocatalytic H_2 evolution rates of the 2.5-Cu_2O/TiO_2 sample with different scavengers (methanol, anhydrous ethanol, ethylene glycol, glycerol) in reaction solution (10 vol%) under UV–vis light irradiation [6]

Thamaraiselvi et al. [1] studied the photocatalytic reduction of carbon dioxide by using bare and copper oxide impregnated nano Titania catalysts. They found that the nanoparticle TiO_2 was synthesized by sol-gel method after that the Copper (Cu) was impregnated over TiO_2 to vary weight percentage (1%, 3%, 5%, 7% and 10% w/w). The bandgap value of CuO impregnated catalyst showed less bandgap values than bare TiO_2. The photocatalytic reaction was tested under 1 atm in closed glass reactor system with a 6W mercury lamp and a 150W tungsten lamp as a light source (UV and visible irradiation). The amount of 0.1 g catalyst was suspended into 100mL of 0.2 M sodium hydroxide after that pure CO_2 gas was purged into the alkali solution until its pH reached 7. The surface area of Degussa P25 is less than the synthesized TiO_2 by sol-gel method therefore, the synthesized TiO_2 catalyst exhibited higher activity than Degussa P25. The 3%CuO/TiO_2 exhibited the optimal photocatalytic activity under UV irradiation because the increased impregnation level of CuO beyond 3%w/w influences to decrease the surface area of TiO_2 and the reduction ability. The yield of formic acid and formaldehyde is maximum irradiation time at 4 hours. The maximum methanol yield is 4,120μmol/gcat at 20 hours after that the catalyst was filtered and dried at 60°C for 24 hours. There is methanol yield 3,900μmol/gcat in second cycle and 3,080μmol/gcat in third cycles. The methanol yield was decreased due to the loss of catalyst particle during filtration. There are yield of methanol 408μmol/gcat, formic acid 0.4μmol/gcat and no formaldehyde under visible irradiation. Both 3%CuO/TiO_2 was oxidized and reduced catalyst to show the less percentage yield of methanol.

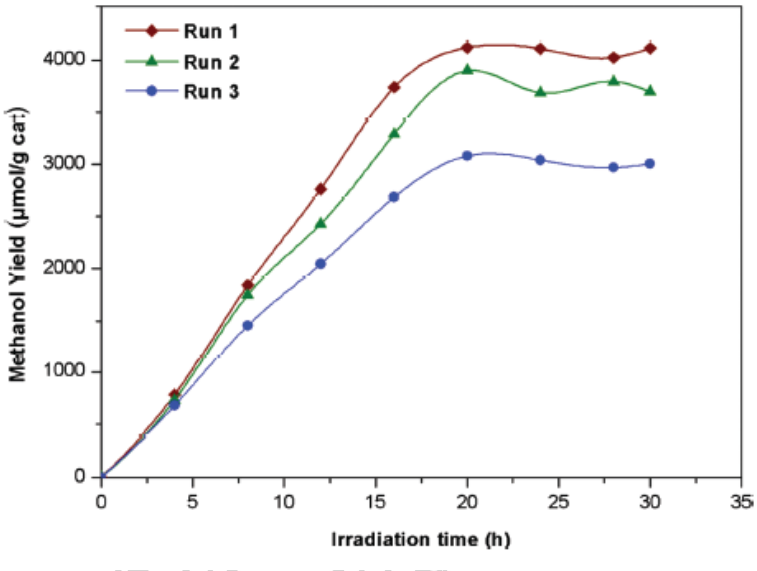

Figure 2: Effect of recycling of 3%CuO/TiO_2 catalyst on the yield of methanol [1]

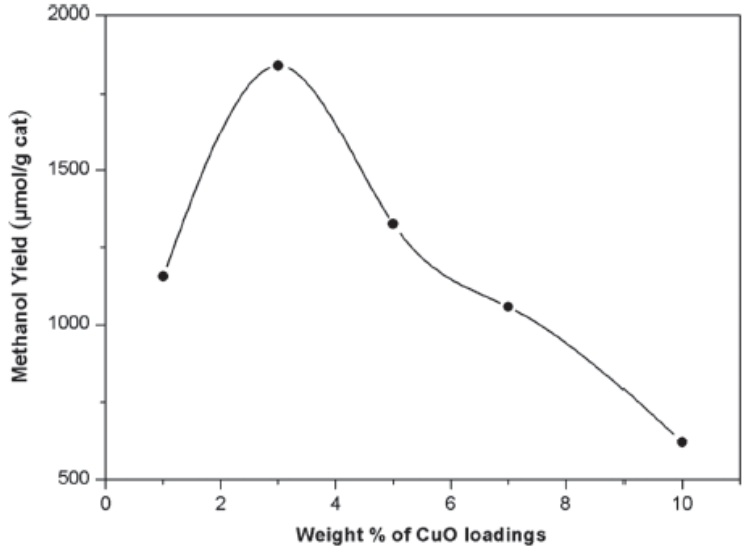

Figure 3: Effect of percentage impregnation of CuO/TiO_2 catalysts on methanol yield [1]

Peng et al. [4] studied the prepared of nitrogen-doped titanium dioxide with visible-light photocatalytic activity using a facile hydrothermal method. They found that The TiO_2 (TiO_2-HT) and Nitrogen-doped TiO_2 (N-TiO_2) nanoparticles were prepared by a direct and simple hydrothermal reaction of a commercial Degussa P25 with tri-ethanol amine (TEA) as a solvent and nitrogen source respectively. The ratio between TiO_2 and TEA is 0.5 g of commercial P25 powder with 40mL TEA solution after that was mixed in a Teflon-lined stainless autoclave. This was tested at 140°C for 24 h. Conclusively, the precipitate was centrifuged and that was dried at 200°C in air for 10 h. The photocatalytic reaction was performed in a 200mL cylindrical glass reactor system with a 1000W Xe lamp as a solar light source about 8% of UV portion. The 20mg of N-TiO_2 catalyst was suspended into 200mL reaction solution by ultrasonicating for 15 min and the reactant is methyl orange dye (MO). The photocatalytic activity of N-TiO_2 is higher than P25 but the lowest photocatalytic activity is TiO_2-HT under solar light because TiO_2-HT can't improve without adding a nitrogen source. The photocatalytic activity of N-TiO_2 is higher than N-TiO_2-NH_3 under visible light on the other hand, the P25 and TiO2-HT were no photocatalytic activity because of wide bandgap energy.

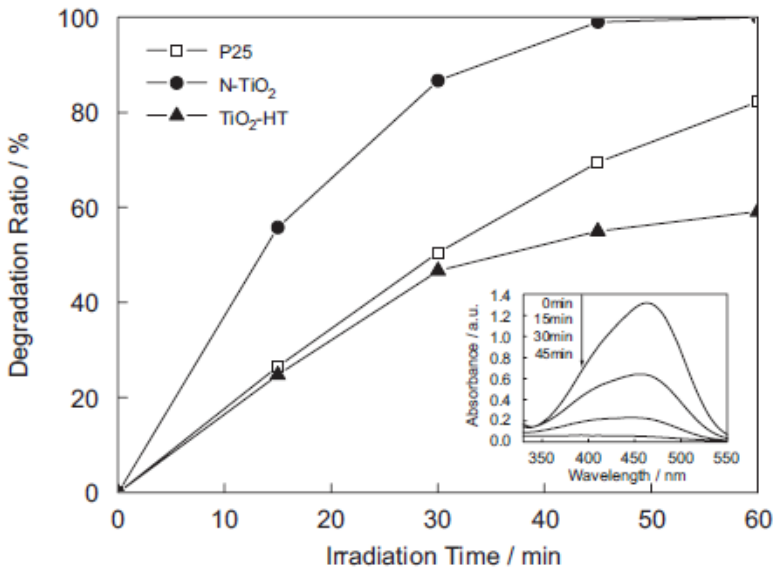

Figure 4: Comparison of the photocatalytic decomposition of methyl orange (MO) under simulated solar light [4]

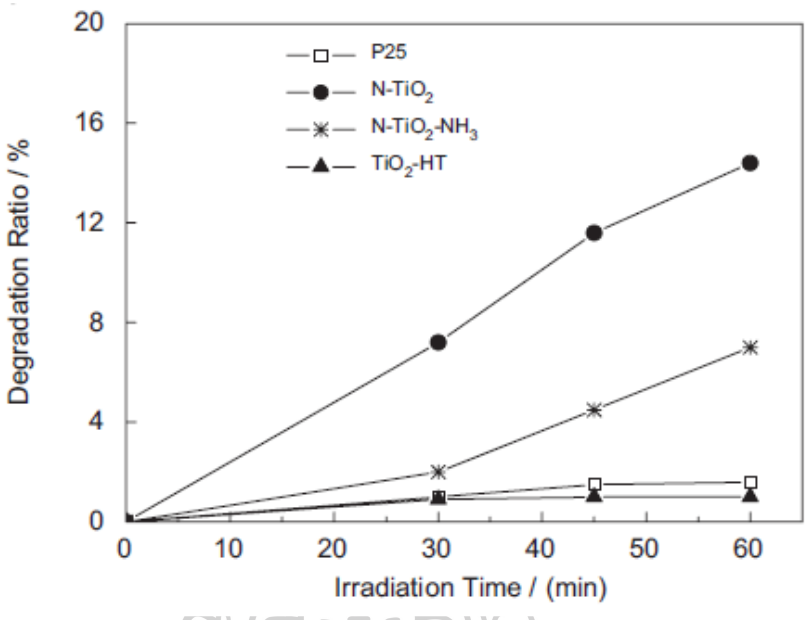

Figure 5: Comparison of the photocatalytic decomposition of methyl orange (MO) under visible light irradiation [4]

Tahir et al. [2] studied gold-indium modified TiO_2 nano catalysts for photocatalytic CO_2 reduction with H_2 as reductant in a monolith photoreactor. They found that the gold-indium modified TiO_2 catalysts were synthesized by sol-gel method. The indium (In) was varied weight percentage (2%, 3.5%, 5%, and 7% w/w) while gold (Au) was used 0.35wt%, 0.5wt% and 0.7wt%. Fixed In-doping 3.5wt% on TiO2 was doped by varied weight percentage of Au (0.1%, 0.2%, and 0.3% w/w). The main product is carbon monoxide (CO) and other product is methane (CH_4). The photocatalytic activity of Au-In/TiO_2 is higher than Au/TiO_2 and In/TiO_2. The monolith that was coated and co-doped monolith catalysts was extracted from the reactor after each cycle.

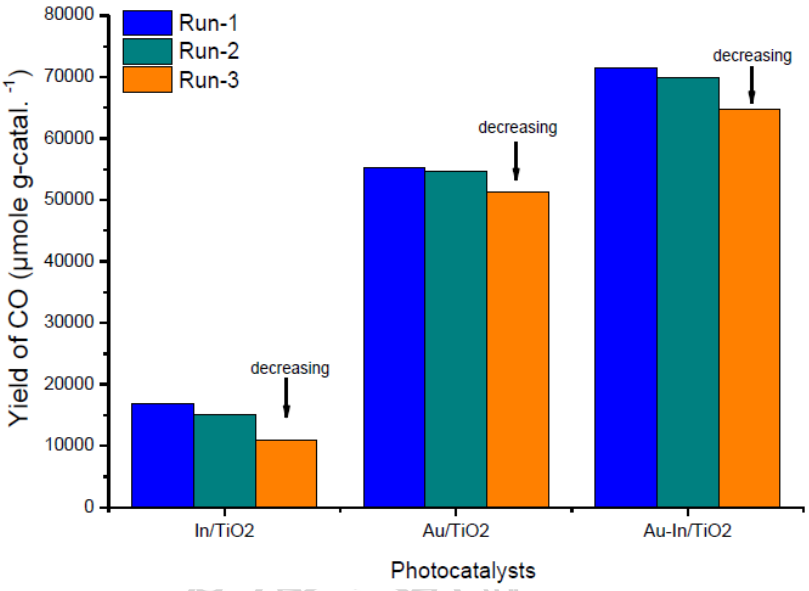

Figure 6: Stability test on photoactivity of 3.5%In/TiO_2, 0.5%Au/TiO_2 and 0.2%Au-3.5% In-co-doped TiO_2 catalyst for CO_2 photoreduction with H_2 to CO at 100°C and CO_2/H_2 ratio 1.5 [2]

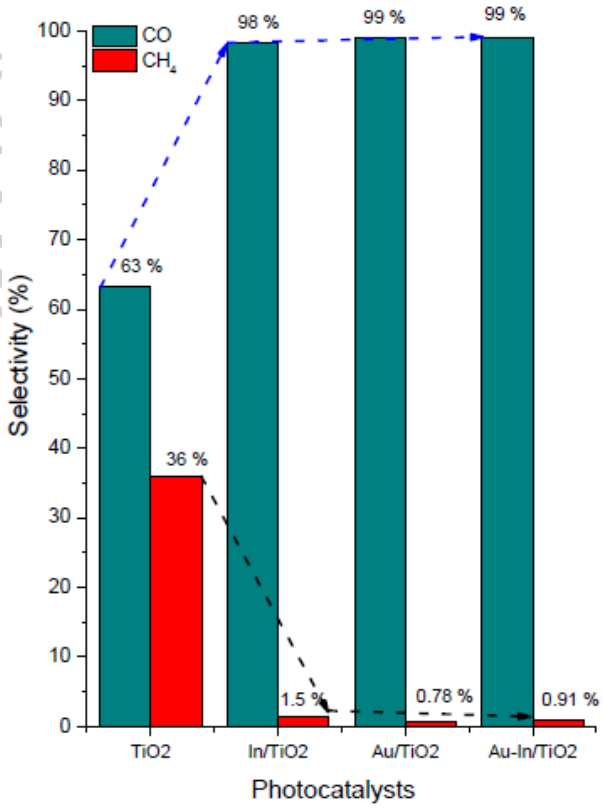

Figure 7: Effects of TiO_2, In/TiO_2, Au/TiO_2 and Au-In/TiO_2 monolithic catalysts on conversion (CO_2, H_4) and selectivity (CO, CH_4) [2]

Meng et al. [3] studied the photocatalytic CO_2 conversion over alkali modified TiO_2 without loading noble metal cocatalyst. They found that the amount of CH_4 photocatalytic was fundamentally improved after increasing NaOH. Amount of NaOH was 3 wt.% and the methane (CH_4) main product was produced 52 mmol/gcat within 6 hours of the reaction. The amount of NaOH (3 wt.%) is a best condition of CO_2 chemisorption. Finally, a reliable reason of CO_2 photoreduction is the surface area of the catalyst.

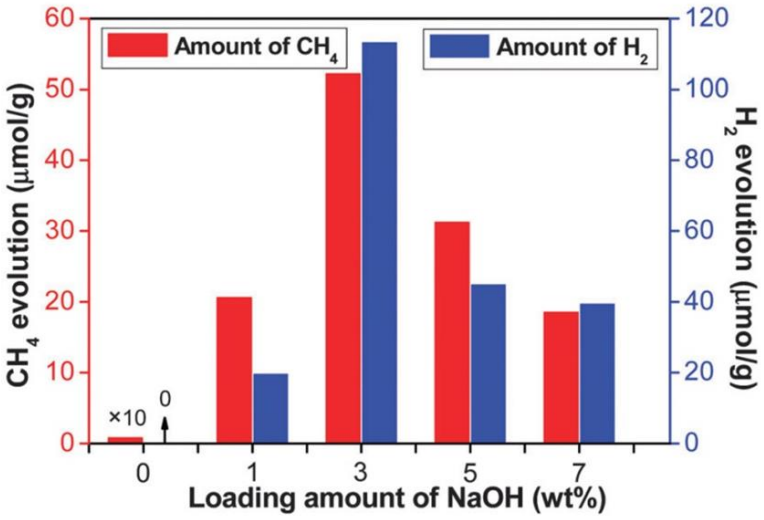

Figure 8: Evolution amounts of CH_4 and H_2 in the first 6 hours irradiation from photocatalytic CO_2 conversion [3]

2.2 Photocatalytic of CO_2 reduction on Ag doped on TiO_2

Krejčíkováa et al. [5] studied preparation and characterization of Ag-doped crystalline Titania for photocatalysis applications. They found that the pure TiO_2 and silver-enriched TiO_2 were synthesized by sol-gel method. The concentration of Silver on TiO_2 (Ag/TiO_2) was varied silver nitrate ($AgNO_3$) solution (0.25M, 0.75M, 1.3M and 1.85M) because that was instead of distilled water during catalyst preparation. The photocatalytic reaction was performed under 1 atm in a stirred batch annular reactor system with 8W Hg lamp (254 and 365nm) as a light source. The amount of 0.1 g catalyst was suspended into 100mL of 0.2 M sodium hydroxide (NaOH) after that pure CO_2 gas was purged into the reactor at room temperature and pH7. The surface area of Degussa P25 is less than the Ag doped sol-gel TiO_2 catalysts process therefore they exhibited higher activity than Degussa P25. The Ag doped sol-gel TiO_2 could reduce the bandgap energy and decreased the electron-hole recombination rate. The 5.2wt%Ag/TiO_2 exhibited the optimal photocatalytic activity under the lamp with wavelength at 254nm. There are 2 main products that yield is methanol 2μmol/gcat and methane 10.5μmol/gcat under the lamp of 254nm. The effect of silver doping on TiO_2 catalyst was tested for the photocatalytic reduction of CO_2. The lamp for this condition is wavelength at 254nm on the other hand, the effect with the lamp of 365nm wavelength was not confirmed.

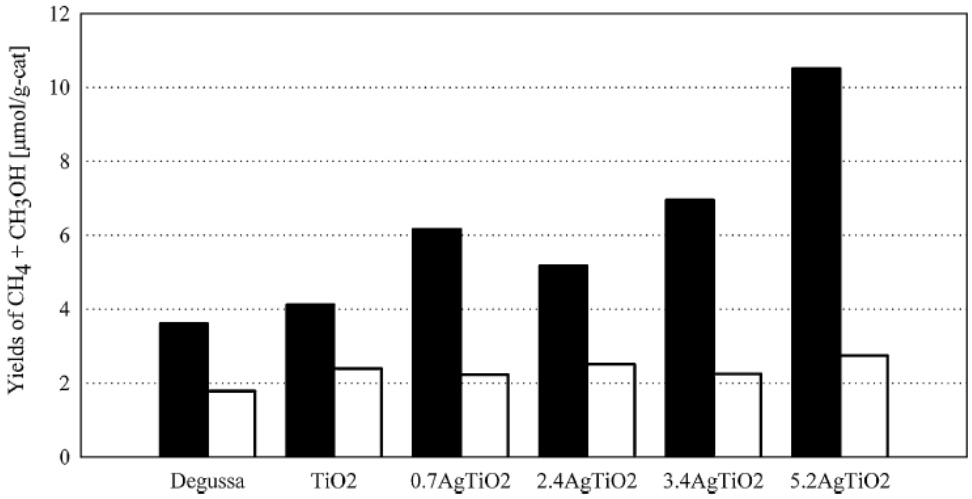

Figure 9: Sums of methanol and methane yields of all prepared and Degussa catalysts; 254nm lamp – dark, 365nm lamp – light [5]

Kočí et al. [33] studied effect of silver doping on the TiO_2 for photocatalytic reduction of CO_2. They found that the pure TiO_2 and silver-enriched TiO_2 were synthesized by sol-gel method. Silver on TiO_2 (Ag/TiO_2) was varied silver nitrate (AgNO3) solution of concentration during catalyst preparation. The photocatalytic reaction was performed in a stirred batch annular reactor system with 8W Hg lamp as a light source. The catalyst of 1 g/dm^3 was loaded into 100mL at room temperature under 1 atm. The 7wt%Ag/TiO_2 exhibited the optimal photocatalytic activity under 254nm lamp. The main product yields that is a methane and methanol are depended on amount of Ag loading on TiO_2 and other product is formic acid, formaldehyde, ethane, and ethylene. The real Ag content of 7wt%Ag/TiO_2 was determined by XRF that there is 5.19wt%. There are yield of methanol 9μmol/gcat and methane 8.5μmol/gcat under the lamp of 254nm. There are two mechanisms for explaining the effect of silver doping on TiO_2 catalyst: first, the matter of Ag atoms scattering on TiO_2 crystals (up to 5%) was affected by more effective electron hole pair generation due to shift of absorption edge towards visible light [33] and one more reason, the mechanism from a Schottky barrier at the metal-semiconductor interface around Ag metallic clusters [34]. This causes spatial separation of electron and holes and decreases their recombination rate.

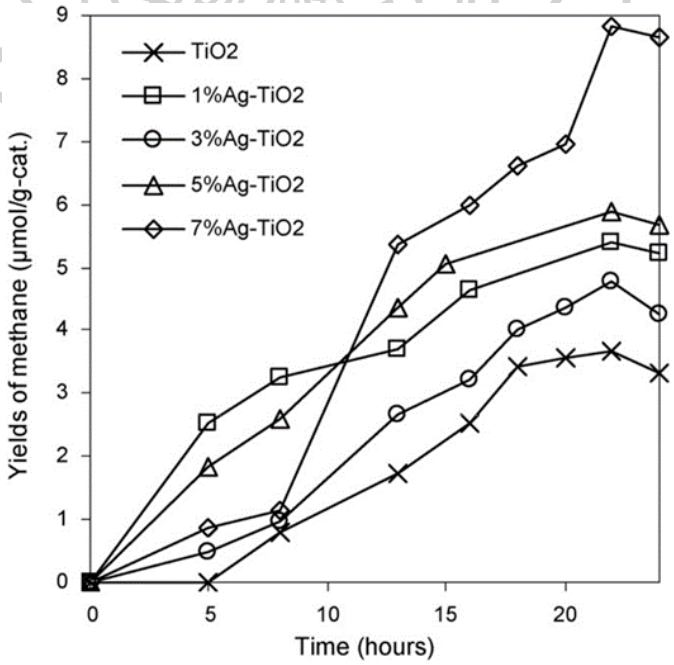

Figure 10: Time dependence of methane yields over the Ag-modified TiO_2 catalysts [33]

Zhao et al. [35] studied ultrasonic spray pyrolysis synthesis of Ag/TiO_2 nanocomposite photocatalysts for simultaneous H_2 production and CO_2 reduction. They found that the optimal concentration of Ag on TiO_2 is 2 wt.% and it was prepared by ultrasonic spray pyrolysis process. For liquid hydrocarbon fuel production, the final product selectivity of H_2/CO ratio lowest and negligible CH4 is in the Fischere-Tropsch process. The electrons and protons in the photocatalytic reaction were competed for H_2 production and CO_2 reduction processes. The ultrasonic spray pyrolysis method is convention for wet impregnation process with the advantages of smaller Ag nanoparticles because the ultrasonic spray pyrolysis method leads to Ag dispersion on TiO_2 and a higher fraction of metallic Ag species better than wet impregnation method. This cause resulted in good photocatalytic activity.

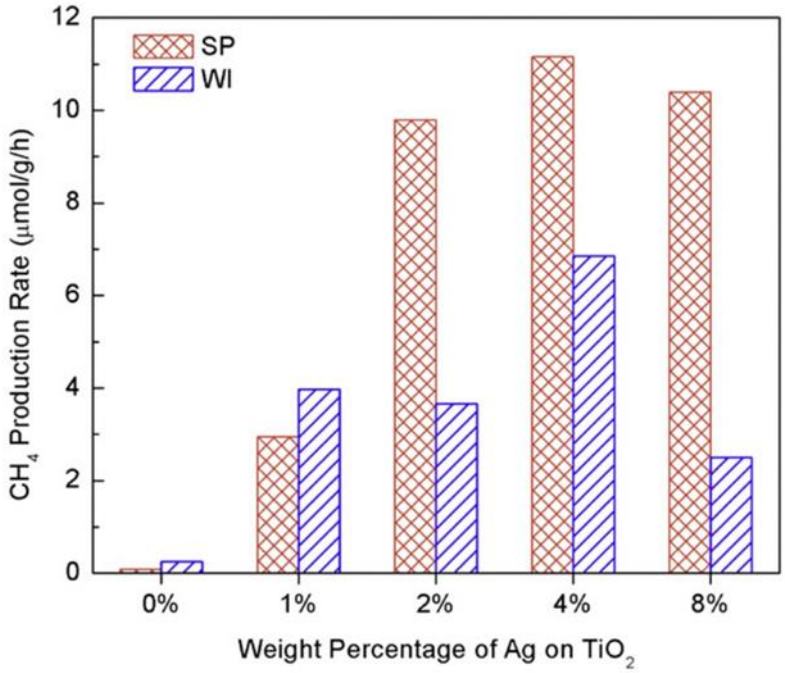

Figure 11: Rates of photocatalytic CO_2 reduction to CH_4 (b) for Ag/TiO2 eSP and Ag/TiO_2 eWI samples at different Ag concentration [35]

Yu et al. [36] studied photocatalytic reduction of CO_2 over Ag/TiO2 nanocomposites prepared with a simple and rapid silver mirror method. They found that the Ag doped on TiO2 nanocomposite was prepared by a simple and rapid silver mirror reaction. The 1.5wt%Ag/TiO_2 showed the optimal photocatalytic reaction. The effect of increasing Ag loading on TiO_2 from 1.0wt% to 1.5wt% leads to an accumulation of electron. However, the Ag loading on TiO_2 was increased to 2.0wt% which the generation rate was decreased to 1.17mol/g.h CH_4. The effect may be happened from the quality factor of the plasmon resonance because the Ag is directly related to the photocatalytic activity.

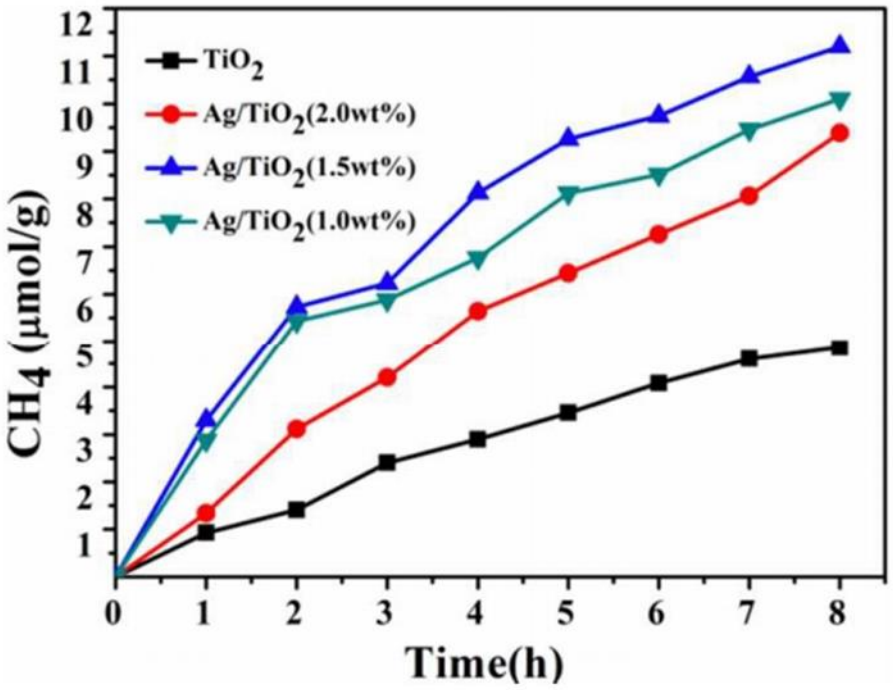

Figure 12: CH_4 evolved during the photocatalysis using pure TiO_2 and 1, 1.5, 2.0 wt% Ag/TiO_2 under UV-visible irradiation in gas phase photoreaction [36]

2.3 Preparation by Flame spray pyrolysis

Flame spray pyrolysis (FSP) is generally known as a method for making nanoparticles such as fume silica, Titania, and carbon black in large quantity at low cost [37]. It is a relatively new process for one-step synthesis of supported metal catalysts. The nanoparticles were generated by the FSP have shown high purity, controlled stoichiometry and metal crystalline because the flame could be maintained at high temperatures [38]. FSP was appeared an attractive fast and single step catalyst preparation method [39].

Gunawan et al. [40] studied reversible antimicrobial photoswitching in nanosilver. They found that the 5 at% Ag/TiO_2 nanoparticles were prepared by the FSP of titanium tetraisopropoxide and silver benzoate co-dissolved in acetonitrile/xylene mixture. The dispersed silver nanoparticle on semiconductor support (TiO_2) was synthesized in a one-step of flame spray pyrolysis (FSP) of silver benzoate and titanium isopropoxide co-dissolved in acetonitrile/xylene. This research used this technique because the FSP is a proven scalable and large production for the synthesis of high-quality nanoparticles or fine particles.

Teoh et al. [41] studied a perspective on the flame spray synthesis of photocatalyst nanoparticles. He found that Flame spray pyrolysis (FSP) include Pt/TiO_2, Ag/TiO_2, Au/TiO_2 and Ag/ZnO. The noble metal has relatively low boiling and sublimation point of the metal compared to oxide photocatalyst that is the first segregation of the noble metals as nanosized deposits during FSP. After that, the former precipitates at a later stage in the flame after the precipitation of the oxide photocatalyst support was low solubility of the two phases which in a different way improved bulk doping rather than surface deposition.

Mekasuwandumrong et al. [37] studied influence of flame conditions on the dispersion of Pd on the flame spray-derived Pd/TiO_2 nanoparticles. They found that the one-step flame spray pyrolysis (FSP) is a method for synthesized 5wt%Pd/TiO_2 under different flame conditions. These catalysts were characterized by X-ray diffraction (XRD) and transmission electron microscopy (TEM). The results of Pd/TiO_2 about an average particle sizes of were increased from 9.7 to 24.6 nm when increasing the precursor concentration and feed flow rate as well as reduction of the

O_2 dispersing gas during FSP synthesis. The amounts of CO chemisorption were higher on the larger size FSP-made Pd/TiO_2 nanoparticles showed %Pd dispersion that Pd/TiO_2 particle size was increasing on the other hand the BET surface area and %anatase phase content was decreased. The shorter residence time in flame and the lower combustion energy (enthalpy density) caused Pd coved on surface more than before. It is suggested that the formation of Ti–O groups.

CHAPTER III

THEORY

This chapter provided some background information necessary for this study such as the synthesis of catalyst by dry impregnation and flame spray pyrolysis (FSP), The CO_2 photocatalytic reduction and the photocatalyst. The details were detailed as follow.

3.1 Dry impregnation

Dry impregnation or incipient wetness impregnation is a principal technique for preparation or synthesis of a heterogeneous catalyst. Dry impregnation shows schematically in Figure 13. Normally, the metal precursor was dissolved in a solution or deionized water after that it is dropped to a support catalyst. The feature of a support catalyst likes a powder. The pore of support catalyst was filled by metal containing solution. The volume of this solution equals a pore volume of a support catalyst. The capillary action is a metal solution to be adsorbed into a pore of catalyst. The metal solution is adsorbed until the pore volume is saturated or excessed. The texture of catalyst is similar to mud or sticky and the capillary action is slower than initial. After that the catalyst is dried and calcined to eliminate the volatile components within the solution. So, the metal is deposited on a surface of support catalyst. The concentration of metal coated on support catalyst is depended on mass transfer condition of pore catalyst [42].

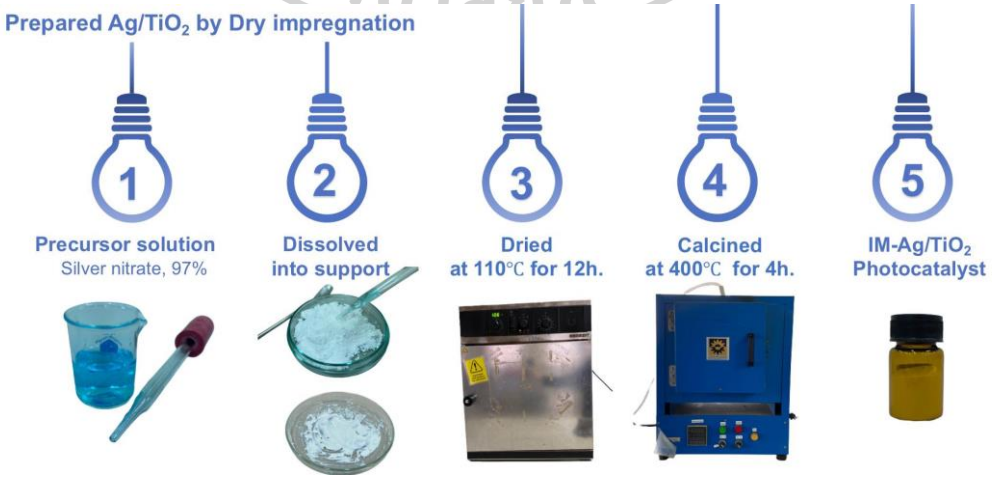

Figure 13: The procedure of dry impregnation

3.2 Flame spray pyrolysis

Flame spray pyrolysis (FSP) is synthesis method of catalyst that can prepare nanostructure powder with high specific surface area in one step process and high catalytic performance [42]. No post-production treatment step requires, and the nanoparticles are ready to use. The nanoparticle is prepared by this method such as fume silica, titania and carbon black in large quantity at low cost [41].

Flame spray pyrolysis (FSP) shows schematically in figure 14 which uses for the synthesis of metal oxide and doped metal oxide particles. The combustion of the precursor solution is sprayed droplets which is used as the basis for the preparation of a compound oxide nano powder. In the middle of the device was fed the precursor solution through a capillary. An annular aperture around the capillary tube is used for liquid feed through a middle of capillary that this liquid feed is atomized under high pressure dispersion gas. The organometallic precursors decomposition and the organic compounds undergo complete combustion was made by methane mixed with oxygen flame let ignites the aerosolized precursor solution under high temperature flame. The primary particles form of pure metals or oxides was nucleated and condensate by the metallic or semi-metallic components of the precursor. The high temperature region of the flame was taking place some aggregation on the other hand quenching owing to productive radiation and convection quickly stops the sintering [43]. Accordingly, the primary particles are going to remain small particle though they do form loose agglomerates in the gas stream owing to high particle concentration and during powder collection [43]. Flame spray pyrolysis (FSP) can produce nanoparticle metal in 1-200 nm by using a substrate that is unexpansive and affordable. It was controlled the production rate of up to 250 grams/hour. The amount and rate of production is depended on conditions. The particle formation and configuration were prepared by FSP. The mechanism in the synthesis transits from a state to gas or vapor particle (gas to particle conversion) or aqueous aerosol droplets into particles (droplet to particle conversion). These are a fundamental process in this synthesis technique. In this section, we further review these particles from in sequential stages of spray

formation, droplet evaporation, nucleation and condensation, coagulation and growth by coalescence and particles aggregation.

After synthesis, obtained particles are retained on the filter paper with special heat resistant properties. The spray of aerosols from the initial solution occurs the formation of the flame of a gas that helps to ignite the methane and oxygen. This will cause the evaporation and combustion of aerosols. Also, using oxygen distributes of the aerosols spray (O_2 dispersion) and controls the oxidation state (O_2 sheet gas) to perfect. Fuel supports the methane gas in system. There is a separate flow control that is clearly out of the box solution to the initial spray. All the gas flow rates were controlled by mass flow controller in the aerosol was changed status quickly. Therefore, the substrate solution into the system will allow the direct reaction with gaseous oxidant oxygen species.

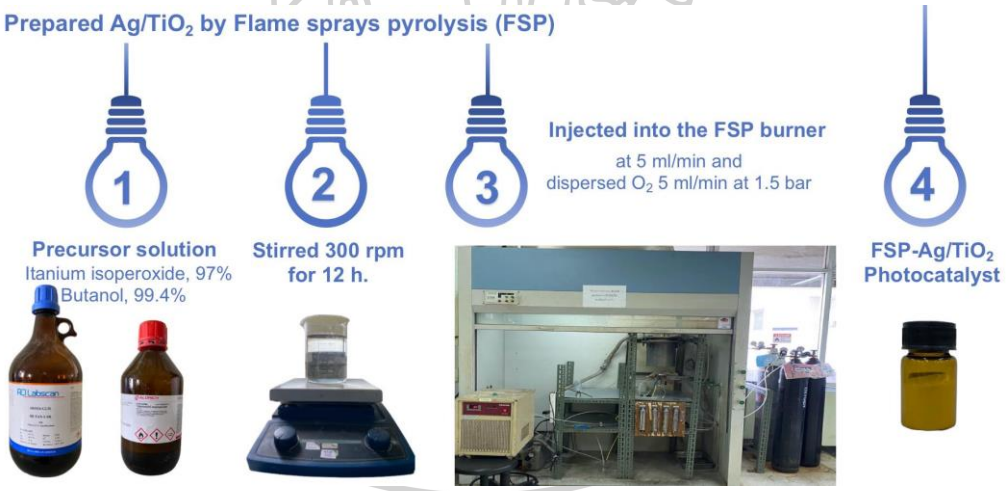

Figure 14: The procedure of Flame spray pyrolysis (FSP)

3.3 CO_2 photocatalytic reduction of TiO_2 and Ag/TiO_2 photocatalyst

The photocatalysis process has been widely investigated. To choose titanium dioxide (TiO_2) as a photocatalyst is nontoxic, abundant, high stability and low cost [44, 45]. Table 3.1 lists some physical properties of rutile, anatase and brookite [39, 46, 47]. Titanium rutile phase and anatase phase exhibited physical properties that slight differences exist. A band gap of both Titanium phases is 3.0–2.3 eV that is affect about reflect visible light while Titanium anatase phase was reflected covering long-wave ultraviolet (UVA) light and visible light as a wider electromagnetic wave. The physical property of Titanium rutile phase absorbs violet visible light on the other hand anatase phase absorbs UVA region to show photo-reduced catalytic effects. Figure 15 shows crystallographic structures of rutile and anatase.

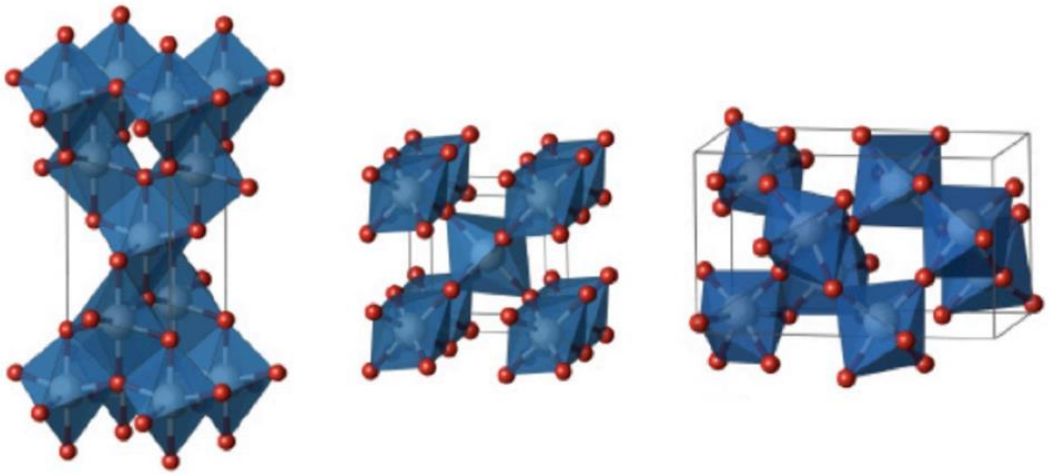

(a) (b) (c)

Figure 15: Crystallographic structure of (a) Anatase, (b) Rutile and (c) Brookite

Table 1: Physical properties of titanium dioxide [48]

Material	Anatase	Rutile	Brookite
Composition	TiO_2	TiO_2	TiO_2
Chemical formula weight	79.87	79.87	79.87
Crystal structure	Tetragonal	Tetragonal	Orthorhombic
Temperature (°C)	25	25	25
a (Å)	3.7842	4.5845	9.184
b (Å)	3.7842	4.5845	5.447
c (Å)	9.5146	2.9533	5.145
α (deg)	90	90	90
β (deg)	90	90	90
γ (deg)	90	90	90
Unit cell volume (Å)^3	136.25	62.07	257.38
Density (g/cm^3)	3.895	4.2743	4.123
Molar volume	20.156	18.693	19.377

The electron of the valance band of TiO_2 is excited by energy and the photocatalysis mechanism diagram of TiO_2 shows on figure 16. The ultraviolet radiation was generated from sunlight or illuminated light source (fluorescent lamps) as an energy. This energy produces the pairs of electrons and holes. The electron is excited by energy when this energy has more than band gap energy. The excess energy of this excited electron led to the conduction band [49] from valance band of TiO_2 because that is produced a negative-electron and positive-hole (Eq. (1)). This stage is appeared with semiconductor photocatalyst. The main issue in the use of TiO_2 is related to low efficiency. The efficiency is limited for activated wavelength because the wide band gap is ~3.2eV that there is only 3-5% of the total solar radiation [50, 51]. The efficiency of semiconductor catalyst is modified by in two ways: doping transition-metal, non-metal or combination. Non-metal is Nitrogen-doped [52, 53], Carbon-doped [54, 55], Fluorine-doped [55, 56], Sulfur-doped [55, 57], Nitrogen-Carbon co-doped TiO_2 [55, 58], transition-metal is Platinum [59, 60], Silver

[27, 30, 33, 36, 61, 62], Copper [63] and Vanadium [64] or combination is Nitrogen-Platinum co-doped TiO_2 [55, 65] and Fluorine-Iron co-doped TiO_2 [45, 55]. The UV illumination for the energy source excited the electron that is excited from valance band to conduction band. This step led to raise electron hole. The water or other molecule that there are a lot of electron or give an electron to is an electron donor (Eq. (2) - (3)). The electron is attached by an electron donor that the function of an electron donor prevents an electron to turn back to hole. In an aqueous solution, the photocatalysis process generated to transfer the electron and instantly reacted with oxygen to form superoxide radicals (O_2^{-o}). The positively charged hole built the hydroxyl groups to form hydroxyl radicals (HO_2^o) or hydrogenperoxide (H_2O_2). The superoxide free radicals and hydroxyl radicals are built at the same time (Eq. (4)-(9)). The properties of these are a high oxidizing ability because of sensitivity. These free radicals degraded solvent into the small molecules [67]. The photocatalysis process consists of the process of transferring the charge of the carrier to organic matter while absorbing the organic matter on the semi-conducting substance. This is considered to reduce the combination of electrons and holes that causes loss of work efficiency during the merging of electrons and holes. It will heat out (Eq. (10)).

$TiO_2 + hV \longrightarrow e^-_{(CB)} + h^+_{(VB)}$ ----(1)

$H_2O + h^+_{(VB)} \longrightarrow OH^o + H^+$ ----(2)

$h^+ + OH^- \longrightarrow OH^o$ ----(3)

$O_2 + e^-_{(CB)} \longrightarrow O_2^{-o}$ ----(4)

$O_2^{-o} + H^+ \longrightarrow HO_2^o$ ----(5)

$2HO_2^o \longrightarrow H_2O_2 + O_2$ -----(6)

$H_2O_2 + O_2^{-o} \longrightarrow OH^- + OH^o + O_2$ -----(7)

$H_2O_2 + e^- \longrightarrow OH^- + OH^o$ -----(8)

$H_2O_2 + hV \longrightarrow 2OH^o$ -----(9)

$e^- + h^+ \longrightarrow TiO_2 + heat$ ---(10)

$TiO_2 + hV \longrightarrow e^-_{(CB)} + h^+_{(VB)}$ ----(11)

$e^-_{(CB)} \longrightarrow e^-_{Ag}$ ----(12)

$e^-_{Ag} + hV \longrightarrow e^-_{SPR}$ ----(13)

$h^+_{(VB)} + H_2O \longrightarrow OH^o + H^+$ ----(14)

$CO_2 + 6e^-_{SPR} + 4H^+ \longrightarrow CH_3OH + 0.5O_2$ ----(15)

The Ag-coated TiO_2 was synthesized by dry impregnation or FSP which demonstrated outstanding efficiency in photocatalytic degradation. Figure 17 shows the excitation–enhancement synergistic mechanism for photocatalytic reduction of CO_2 on Ag/TiO_2 composite [16]. The high photocatalytic activity in TiO_2 can be ascribed to Ag because that decreases the recombination rate of electron-hole pairs.

Eq. (11) – (15) showed the process of photocatalytic reduction CO_2. The photoreaction of the Ag/TiO_2 composite is participated about the electrons and holes on the surface photocatalyst [16]. The H_2O or OH^- to form hydroxyl radicals (·OH) are oxidized by activated h^+ (VB) and O_2 and H^+ like a function of H_2O or OH^- [66]. CO_2 reduction and produced methanol or other hydrocarbons was generated by H^+ and high active e^-_{SP} [67, 68]. The six e^-_{SPR} are required to convert the C^{4+} of CO_2 into C^{2-} of CH_3OH was indicated by Equation (15). Ag nanoparticles play a crucial role in the above process for electron trapping was apparated by it in the same way surface plasmon resonance (SPR) enhancement [69].

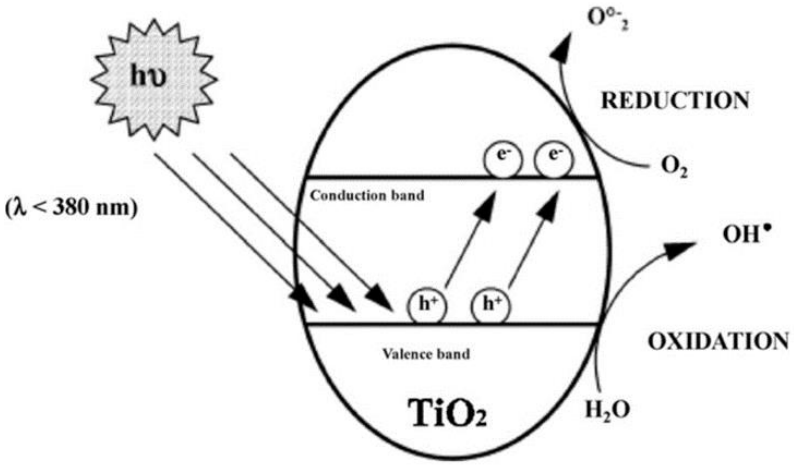

Figure 16: The photocatalysis mechanism diagram of TiO_2 [70]

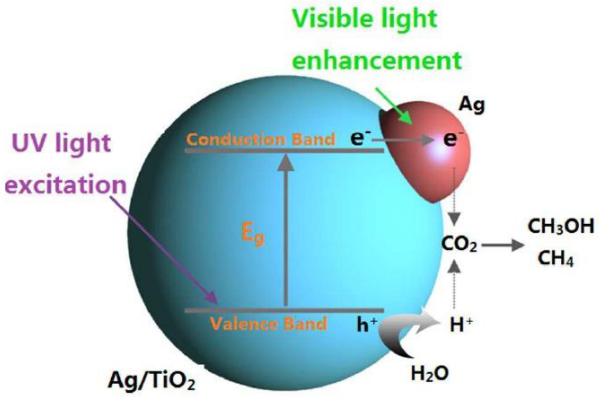

Figure 17: The excitation–enhancement synergistic mechanism for photocatalytic reduction of CO_2 on Ag/TiO_2 composite [36]

CHAPTER IV

METHODOLOGY

This chapter describes the experimental procedures for synthesis of TiO_2 and Ag/TiO_2 for CO_2 photocatalytic reduction reaction. This chapter consists three parts. The first part explains the materials and the preparation method of nanoparticles by dry impregnation and flame spray pyrolysis. Second part shows the details of characterization techniques. Finally, show the reaction evaluation for CO_2 photocatalytic reduction.

4.1 Materials

The chemicals were used in this research that shows in Table 2 as a precursor for catalyst preparation (Flame spray pyrolysis and Impregnation method).

Table 2: The details of chemical were used in the catalyst preparation.

Chemical	Formula	Grade	Suppliers
Titanium (IV) isopropoxide	$Ti\{(OCH(CH_3))_2\}_4$	97%	Sigma-Aldrich
Titanium (II) oxide	TiO_2	P25 grade	Chula University
Butanol	C_4H_9OH	99.4%	Labscan
Methanol	CH_3OH	99.4%	Sigma-Aldrich
Silver (I) nitrate	$Ag(NO_3)$	99.5%	Merck
Sodium hydroxide	NaOH	97%	KEMAUS

4.2 Catalyst preparation

4.2.1 Preparation of Ag/TiO_2 catalyst by Dry impregnation

It was prepared by dry impregnation. First, the silver was dissolved and dropped into TiO_2 support catalyst until it saturates because of calculate the total pore volume from this step. Second, the thick slurry was dried at 110°C overnight after that the powders were calcined at 400°C 4 hours. The content of Ag was varied 1wt%Ag, 3wt%Ag, 5wt%Ag and 7wt%Ag. The procedure of dry impregnation shows in Figure 13.

4.2.2 Preparation of TiO_2 and Ag/TiO_2 catalyst by Flame sprays pyrolysis method

TiO_2 non-loading

Titanium (IV) butoxide was dissolved in xylene. The content of bare Titanium (IV) butoxide obtains the final FSP nanoparticles precursor solution.

Ag loading on TiO_2

Silver (I) nitrate and Titanium (IV) butoxide were dissolved in xylene. The content of Pt loading was varied from 1wt%Ag, 3wt%Ag, 5wt%Ag and 7wt%Ag to obtain the final FSP nanoparticles precursor solution. The preparation condition of non-loading and Ag loading on TiO_2 prepared by FSP method was described below. The precursor solution was fed into a flame spray pyrolysis apparatus by a syringe pump. The rate of syringe pump is 5 mL/min of precursor solution that was dispersed into fine droplets by a gas-assist nozzle and fed 5 L/min of oxygen. The orifice gap area at the nozzle was adjusted 1.5 bars because of maintained the pressure drop at the capillary tip. A ring around the nozzle outlet is the position for ignition. The ignited spray was fed 3 L/min oxygen and 1.5 L/min methane for supporting flame. An additional 10 L/min of oxygen as sheath for the supporting flame was provided by a sintered metal plate ring (8 mm wide, starting at a radius of 8 mm) [41]. A glass fiber filter with a vacuum pump used for collected the product particles. The procedure of FSP shows in Figure 14.

4.3 Catalyst characterization

4.3.1 N_2-physicsorption (BET)

N_2-physicsorption was determined textural properties as an average pore size and a pore volume. The 0.1 g of catalyst was pretreated at 180°C for 3 hr. under high vacuum. The Dewar flask was contained liquid nitrogen that the sample port was dipped in it. The volume of N_2 was measured at -196 °C using as the different N_2 partial pressure. Brunauer-Emmett and Teller (BET) used to find specific surface area. Pore volume and pore diameter were calculated by Barret – Joyner – Halenda (BJH).

Figure 18: N_2-physicsorption (Belsorpmini 2)

4.3.2 UV-Visible adsorption spectrometer (UV-Vis)

UV-Vis Spectrophotometer was used to find maximum wavelength and band gap energy (Eg) of photocatalyst. This was absorbed by sample in rang of UVA, UVB, UVC or visible light. LAMDA 650 UV/Vis spectrophotometer was used for measured the UV–vis absorption spectra and band gap energy of sample powders. This spectrophotometer was scanned around wavelength of 200–900 nm and used a UV Win Lab software from Perkin-Elmer.

Figure 19: UV-Vis spectrometer (T92+ UV-Vis spectrometer PG Instruments Limited)

4.3.3 X-ray diffractometer (XRD)

X-ray diffractometer (XRD) was identified the crystal structures, composition and state of crystalline particle by electromagnetic radiation. X-ray diffractometer can identify a crystalline material and provide informative crystal structure. This experiment used diffractometer with CuK_{α} radiation when it performs operation at 40 kV and 30 mA.

Figure 20: X-ray diffraction (Model D8 Advance: Bruker AXS, Germany with CuKα radiation)

4.3.4 Photoluminescence Spectrometer (PL)

The recombination rate analysis by Photoluminescence Spectrometer for excite on wavelength 340 - 550 nm at Faculty of Engineering, Chulalongkorn University.

Figure 21: Photoluminescence Spectrometer (Fluromax® by Horiba and using Xenon lamp source)

4.3.5 Transmission electron microscopy (TEM)

The morphology and catalyst particle size were determined by Transmission electron microscopy (TEM) with bright-field and dark-field and using Olympus TECNAI 20 TWIN Transmission electron microscopy at 120 kV. The samples were dispersed in ethanol as a solution and liquid solution was dropped into a mesh of carbon grid. This was coated by holey carbon and dried on a filter paper before scanning. Th scanning was done many times in difference area because of fine dispersion.

Figure 22: Transmission electron microscopy (Olympus TECNAI 20 TWIN)

4.3.6 X-ray photoelectron spectroscopy (XPS)

The binding energy and surface composition of catalysts was determined by X-ray photoelectron spectroscopy (XPS) with MgK_{α} X-ray source as a primary excitation as the AMICUS photoelectron spectrometer. XPS equipment was get with a 0.1 eV energy step at a pass energy of 75 eV. The controlled software was KRATOS VISION2.

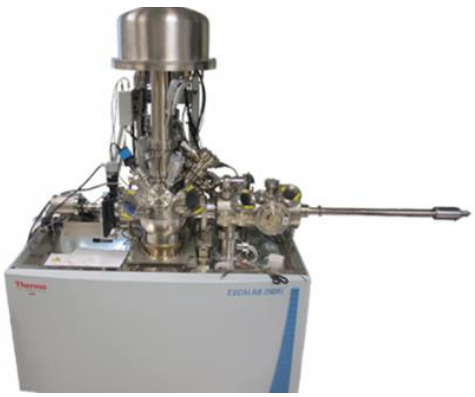

Figure 23: X-ray photoelectron spectroscopy (AMICUS photoelectron spectrometer)

4.4 Reaction test

The photocatalytic reaction was carried out in a gas circulation system and was performed under the set of UV 6 lamps (UV irradiation). The volume of Quartz reactor is 400 cm^3. Photocatalyst for this experiment used 0.3 g with 100ml DI water. The CO_2 gas was purged by a bubble for 30 min with flow rate 100 ml/min after that turned on the lamps and stirred 3 hours under room temperature. The gas production was analyzed by gas chromatograph with a thermal conductivity detector (GC-TCD) and liquid production was analyzed by gas chromatograph with a flame ionization detector (GC-FID).

(1) (2) (3) (4)

Figure 24: The procedure of Reaction test

CHAPTER V

RESULT AND DISCUSSION

The objective of this research focused on the study of effect silver (Ag) metal doped on titanium dioxide. This result showed the physicochemical and photocatalytic properties of pure TiO_2 and Ag/TiO_2 photocatalysts in photocatalytic CO_2 reduction. Therefore, the result and discussion were explained in this chapter that there are two section: physicochemical properties characterization and photocatalytic activity.

Table 3: The specimen designation of the catalysts in this work

Sign	Detail of sign
P25-TiO_2	The TiO_2 commercial catalyst P25 (Degussa)
IM-1wt% Ag/TiO_2	Impregnated Ag doped on P25 catalyst at 1wt%
IM-3wt% Ag/TiO_2	Impregnated Ag doped on P25 catalyst at 3wt%
IM-5wt% Ag/TiO_2	Impregnated Ag doped on P25 catalyst at 5wt%
IM-7wt% Ag/TiO_2	Impregnated Ag doped on P25 catalyst at 7wt%
FSP-TiO_2	Flame spray pyrolysis Ag/TiO_2 catalyst
FSP-1wt% Ag/TiO_2	Flame spray pyrolysis Ag/TiO_2 catalyst at 1wt%
FSP-3wt% Ag/TiO_2	Flame spray pyrolysis Ag/TiO_2 catalyst at 3wt%
FSP-5wt% Ag/TiO_2	Flame spray pyrolysis Ag/TiO_2 catalyst at 5wt%
FSP-7wt% Ag/TiO_2	Flame spray pyrolysis Ag/TiO_2 catalyst at 7wt%

5.1 Physicochemical properties characterization

5.1.1 N_2-physicsorption (BET)

N_2-physicsorption is used to determine the BET surface area, total pore volume and average pore size diameter of all photocatalysts. These results are summarized in the Table 4 and the adsorption/desorption isotherm of all catalysts are exhibited in figure 25-26. The BET surface area of all dry impregnated-made catalysts and FSP-made catalysts exhibited in the range of 40 m^2/g to 56 m^2/g. The total pore volume of all dry impregnated-made catalysts and FSP-made catalysts exhibited in the range of 0.08 cm^3/g to 0.20 cm^3/g. The BET surface area and total pore volume of each dry impregnated-made catalysts and FSP-made catalysts are similarly but total pore volume of all FSP-made catalysts is less than all dry impregnated-made catalysts. Doping with Ag decreases the BET surface area but did not significantly alter the total pore volume and average pore size diameter of dry impregnation-made catalysts. In the same way, doped Ag did not significantly affect in the BET surface area, total pore volume and pore size diameter of flame-made catalysts.

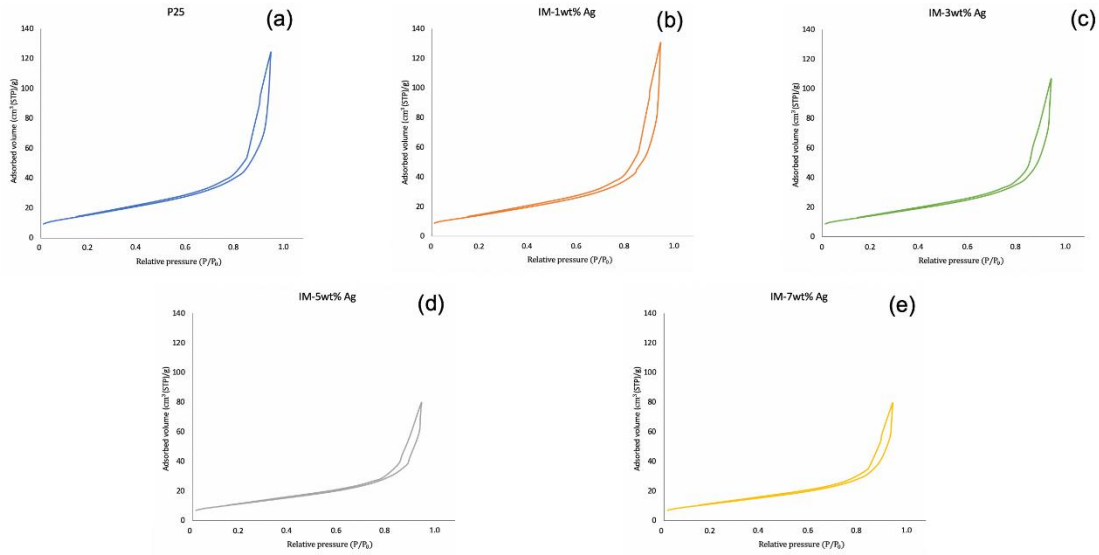

Figure 25: The N_2-adsorption/desorption isotherm of a) P25, b) IM-3wt% Ag/TiO_2, c) IM-3wt% Ag/TiO_2, d) IM-5wt% Ag/TiO_2 and e) IM-7wt% Ag/TiO_2

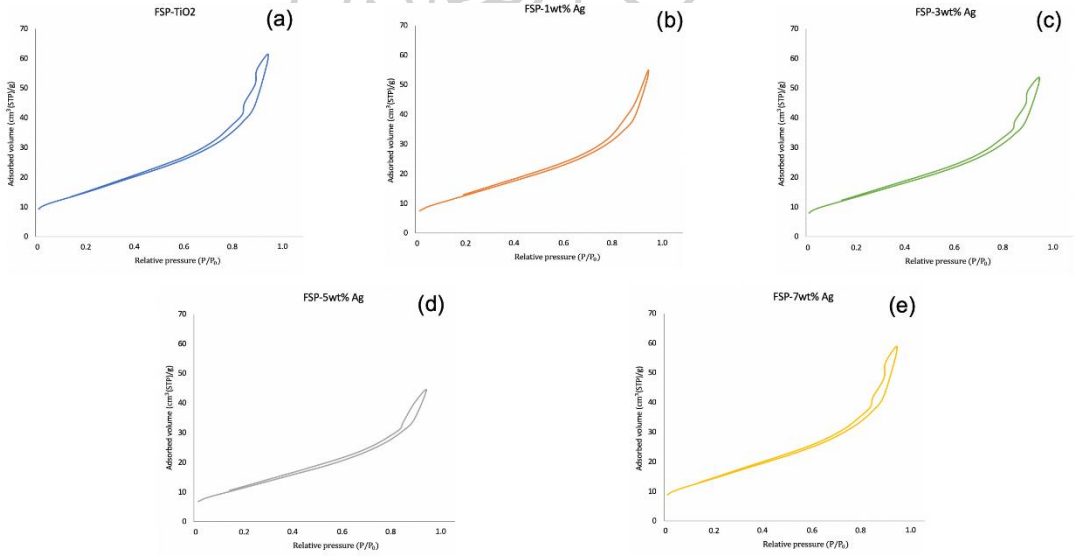

Figure 26: The N_2-adsorption/desorption isotherm of a) FSP-TiO_2, b) FSP-1wt% Ag/TiO_2, c) FSP-3wt% Ag/TiO_2, d) FSP-5wt% Ag/TiO_2 and e) FSP-7wt% Ag/TiO_2

Table 4: The BET surface area, total pore volume and pore size diameter of all photocatalysts

Photocatalysts	S_{BET} (m^2/g)	Pore volume (cm^3/g)	Pore size (nm)	Adsorption isotherms
P25-TiO_2	55.69	0.19	13.78	Macropores Structure
IM-1wt% Ag/TiO_2	52.17	0.20	15.44	
IM-3wt% Ag/TiO_2	50.48	0.16	13.05	
IM-5wt% Ag/TiO_2	41.63	0.12	11.81	
IM-7wt% Ag/TiO_2	40.39	0.12	12.15	
FSP-TiO_2	53.00	0.10	7.20	Macropores Structure
FSP-1wt% Ag/TiO_2	46.79	0.08	7.25	
FSP-3wt% Ag/TiO_2	47.53	0.08	6.98	
FSP-5wt% Ag/TiO_2	42.17	0.07	6.51	
FSP-7wt% Ag/TiO_2	51.22	0.09	7.13	

5.1.2 UV-Vis spectrophotometer

The UV-Vis absorption spectra of all the dry impregnation (IM) and the flame spray pyrolysis (FSP) catalysts were compared with P25-TiO_2 in figure 27-28. Figure 27 shows the UV-Vis absorption spectra of all the photocatalysts prepared by dry impregnation (IM) together with P25 support. There are five photocatalysts including 1wt% Ag/TiO_2, 3wt% Ag/TiO_2, 5wt% Ag/TiO_2, 7wt% Ag/TiO_2 and commercial TiO_2 (P25). UV-Vis bands of photocatalysts showed the sharp absorption band at wavelengths less than 400 nm. The adsorption at the wavelength higher than 400 nm increased after doping amounts of Ag increased. The band structure of commercial TiO_2 was associated with Impregnated Ag doped on P25 catalysts. Figure 28 shows the UV-Vis absorption spectra of the photocatalysts prepared by flame spray pyrolysis (FSP). There are five photocatalysts samples including 1wt% Ag/TiO_2, 3wt% Ag/TiO_2, 5wt% Ag/TiO_2, 7wt% Ag/TiO_2 and pure TiO_2. Similarly, the flame spray pyrolysis catalysts showed the sharp absorption band at wavelengths less than 400 nm. The Increasing of Silver (Ag) doped on FSP-TiO_2 caused the increased of absorbance at the wavelength higher than 400 nm.

The band gap energy (Eg) of IM-photocatalyst and FSP-photocatalyst were showed in Table 5 calculated from figure 29-30. The result of this table was extrapolated from Tauc plots of $(h\nu\alpha)^{1/2}$ as a function of photon energy (hv). The band gap energy (Eg) was decreased owing to increasing of Silver (Ag) doped on TiO_2. The photosensitivity of all photocatalysts and the absorption edge in visible light region (400-700 nm) are improved by decreasing of Eg and Fermi level was reduced due to decreasing of Eg.

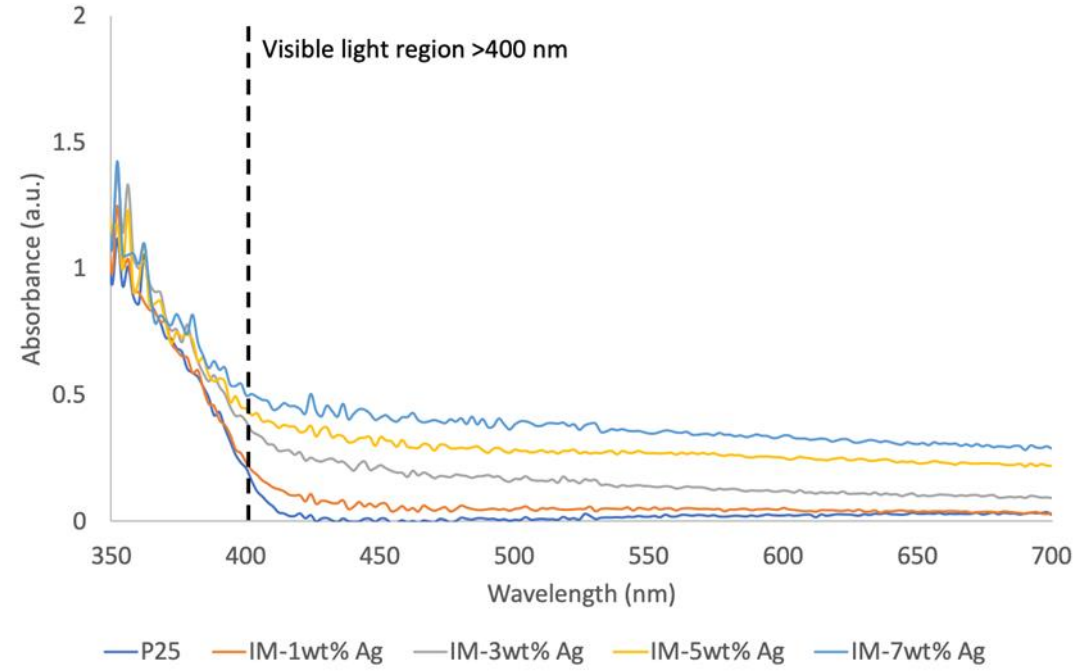

Figure 27: The UV-Vis absorption spectra of IM-Ag/TiO_2 and P25-TiO_2 photocatalysts

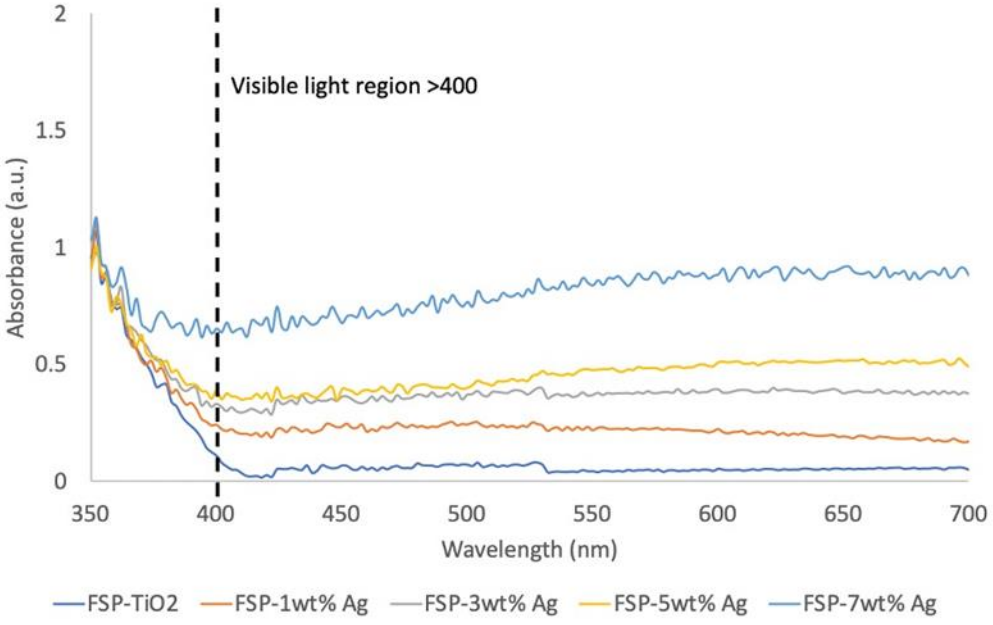

Figure 28: The UV-Vis absorption spectra of FSP-Ag/TiO_2 and FSP-TiO_2 photocatalysts

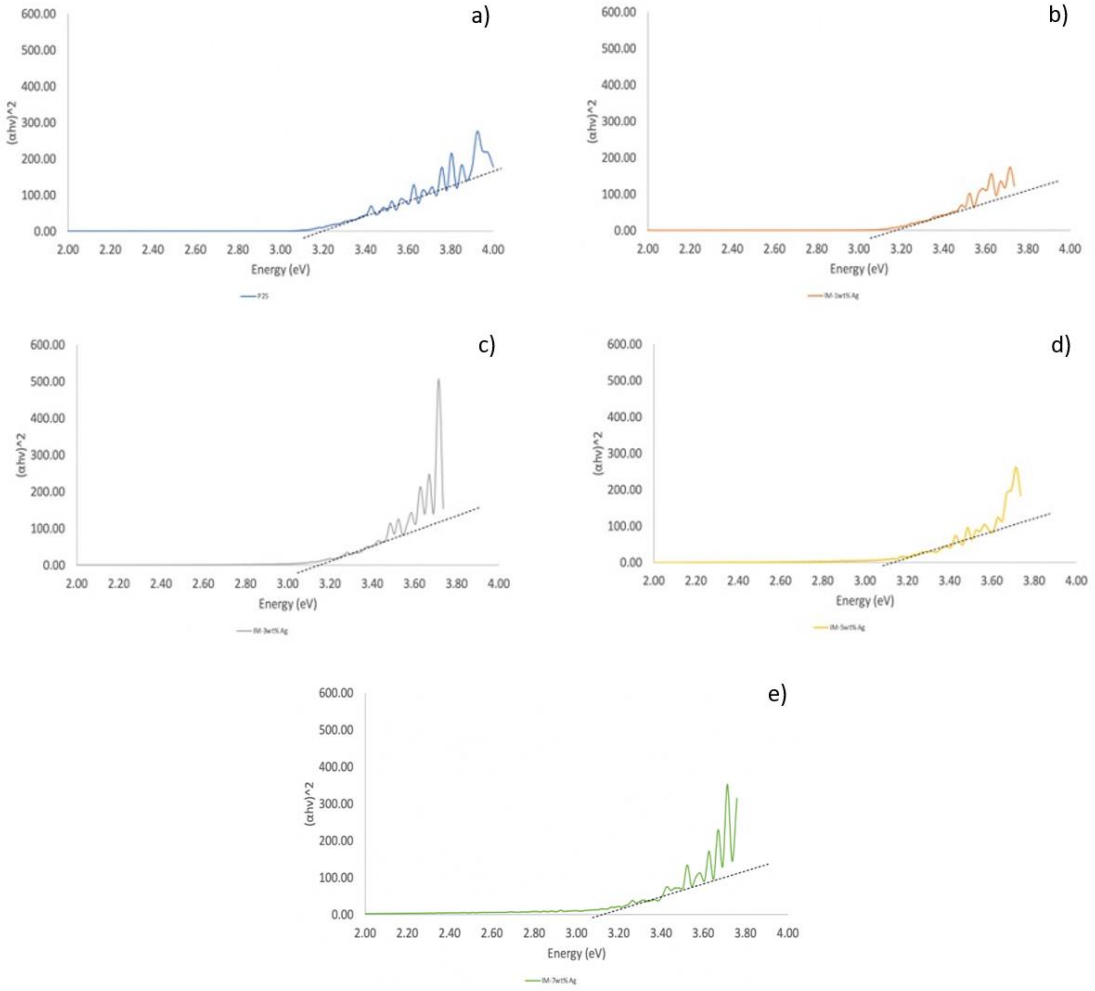

Figure 29: Plot of transformed Kubelka-Munk function versus hV (eV) of a) P25, b) IM-3wt% Ag/TiO_2, c) IM-3wt% Ag/TiO_2, d) IM-5wt% Ag/TiO_2 and e) IM-7wt% Ag/TiO_2

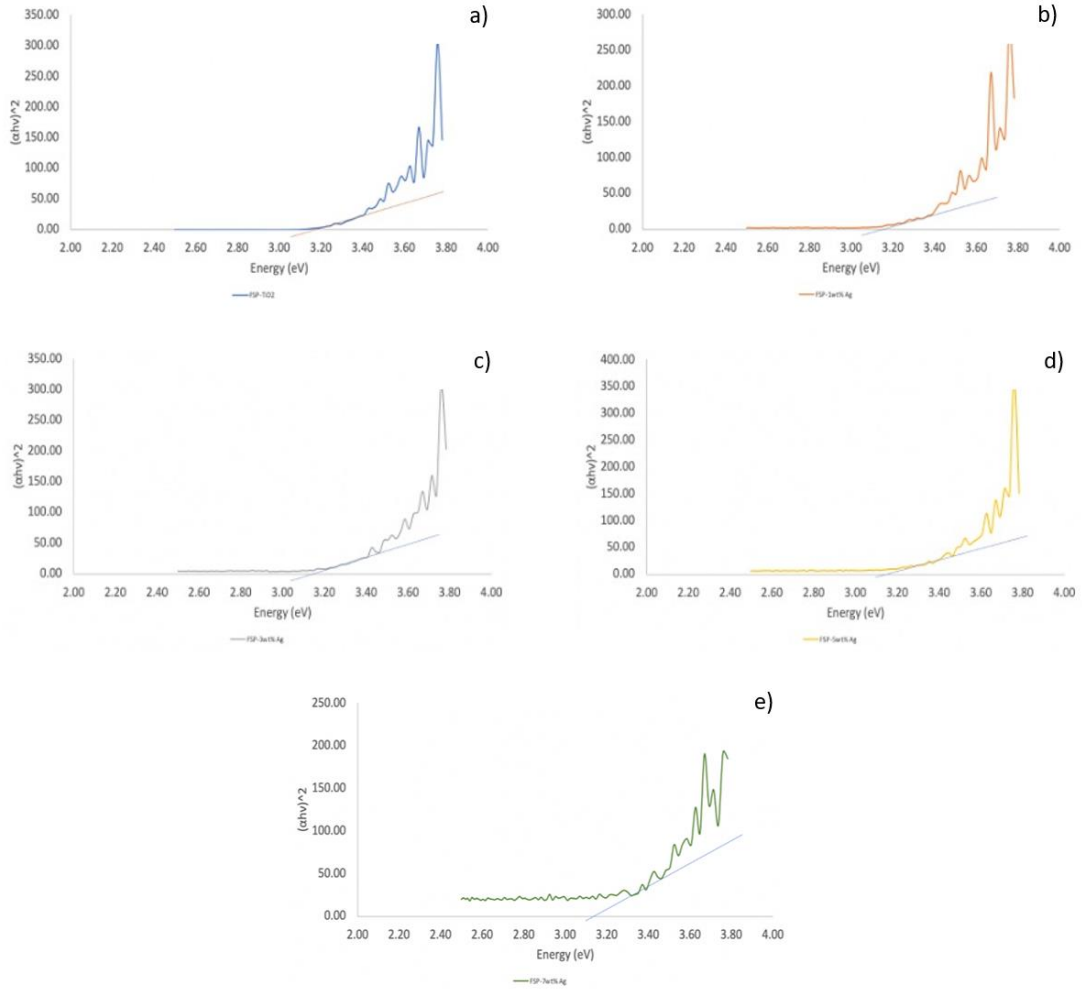

Figure 30: Plot of transformed Kubelka-Munk function versus hV (eV) of a) FSP-TiO_2, b) FSP-1wt% Ag/TiO_2, c) FSP-3wt% Ag/TiO_2, d) FSP-5wt% Ag/TiO_2 and e) FSP-7wt% Ag/TiO_2

Table 5: The energy band gap (Eg) of photocatalysts

Photocatalysts	Energy band gap, E_g (eV)	Photocatalysts	Energy band gap, E_g (eV)
P25-TiO_2	3.20	FSP-TiO_2	3.24
IM-1wt% Ag/TiO_2	3.18	FSP-1wt% Ag/TiO_2	3.16
IM-3wt% Ag/TiO_2	3.14	FSP-3wt% Ag/TiO_2	3.16
IM-5wt% Ag/TiO_2	3.10	FSP-5wt% Ag/TiO_2	3.18
IM-7wt% Ag/TiO_2	3.08	FSP-7wt% Ag/TiO_2	3.14

5.1.3 X-ray diffractometer (XRD)

The XRD pattern of TiO_2 and Ag/TiO_2 photocatalysts were shown in fig 31-32. The diffraction peaks of anatase TiO_2 can be observed at 2θ = 25.3°, 36.9°, 37.9°, 38.5°, 48.0°, 54.9°, 55.0°, 62.1°, 68.9°, 70.3°, 75.1° and 76.0° and the small diffraction peaks of rutile phases was also found at 2θ = 27.36° (110) [71]. All samples, exhibited the peaks mainly of only anatase and rutile TiO_2 phase as a main peak [72]. The characteristic peaks positions of all Ag metal/oxide phases were not observed because of the very high dispersion of Ag phase on both catalysts. However, the FSP-7wt% Ag/TiO2 exhibited the small two peaks at 2θ = 38.2° (111) and 77.6° (311) which are the crystallographic planes of face-centered cubic (fcc) silver crystals [73, 74]. The ratio of pure anatase and rutile phase have been calculated using Debye-Scherrer's equation (see Appendix B) and the results are summarized in table 6.

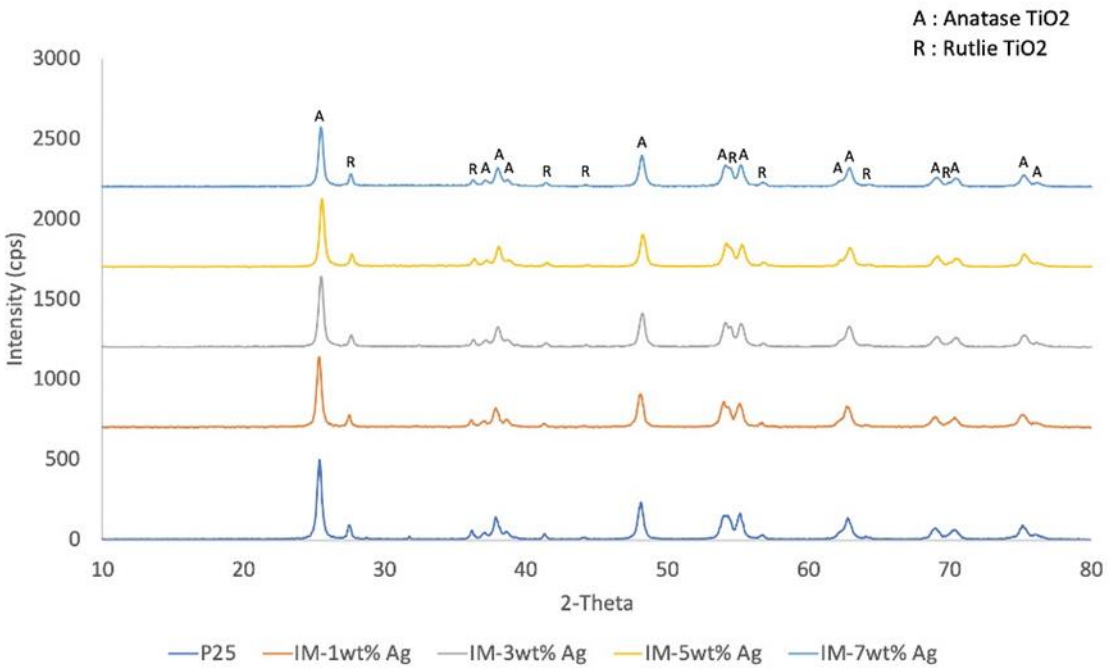

Figure 31: XRD patterns of P25 and IM-Ag/TiO_2

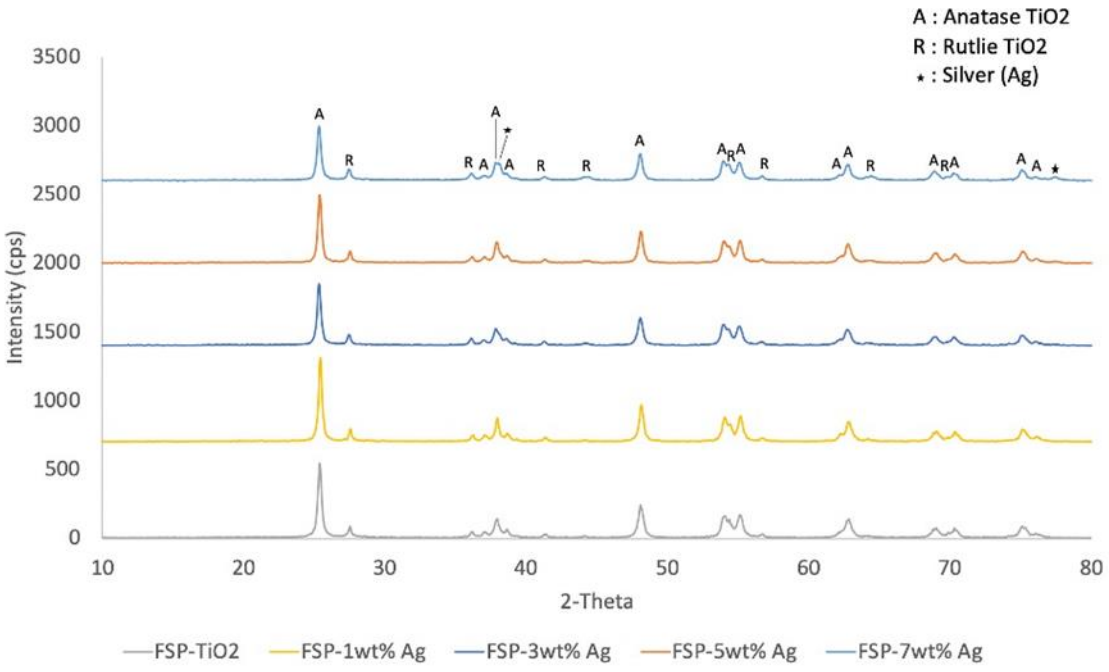

Figure 32: XRD patterns of FSP-TiO_2 and FSP-Ag/TiO_2

Table 6: The crystalize phase and crystalize size

Photocatalysts	Crystalize phase	Crystalize size (nm)	%Compositions
P25-TiO_2	Anatase[1], Rutile[2]	28.49[1], 29.47[2]	80.79[1], 19.21[2]
IM-1wt% Ag/TiO_2	Anatase[1], Rutile[2]	28.49[1], 29.47[2]	81.53[1], 18.47[2]
IM-3wt% Ag/TiO_2	Anatase[1], Rutile[2]	28.49[1], 29.47[2]	81.95[1], 18.05[2]
IM-5wt% Ag/TiO_2	Anatase[1], Rutile[2]	28.49[1], 29.47[2]	80.43[1], 19.57[2]
IM-7wt% Ag/TiO_2	Anatase[1], Rutile[2]	28.49[1], 29.47[2]	78.62[1], 21.38[2]
FSP-TiO_2	Anatase[1], Rutile[2]	28.49[1], 29.47[2]	83.86[1], 16.14[2]
FSP-1wt% Ag/TiO_2	Anatase[1], Rutile[2]	28.49[1], 29.47[2]	83.32[1], 16.68[2]
FSP-3wt% Ag/TiO_2	Anatase[1], Rutile[2]	28.49[1], 29.47[2]	81.69[1], 18.31[2]
FSP-5wt% Ag/TiO_2	Anatase[1], Rutile[2]	28.49[1], 29.47[2]	81.98[1], 18.02[2]
FSP-7wt% Ag/TiO_2	Anatase[1], Rutile[2], Ag	28.49[1], 29.47[2], 2.97	79.25[1], 20.75[2]

5.1.4 Photoluminescence spectrometer (PL)

The PL spectra of the P25-TiO_2, impregnation-made and the flame-made were shown in figure 33-34. The PL emission spectra indicates the electron-hole recombination rate by detecting the release energy from the electron-hole recombination process. The PL emission spectra exhibited many peaks within visible region at around 430nm, 450nm and 470 nm, which were excited under 250 nm. The self-trapped electron on TiO_2 region communicated with the peak around 436nm [75]. The oxygen vacancies with two trapped electrons on TiO_2 surface were indicated at 469, 484 and 492nm [76, 77]. The PL spectra was decreased when Ag doping content increased, whereas the PL spectra of P25 was similar to 1wt%Ag/TiO_2. Increased Ag led to disappeared new emission peak [33]. Figure 34 exhibits the PL emission spectra of Ag/TiO_2 photocatalysts prepared by flame spray pyrolysis (FSP). The PL spectra was decreased by increased of Ag loading. The results suggest that the Ag^+ on conduction band of TiO_2 leads to decrease the electron-hole recombination rate.

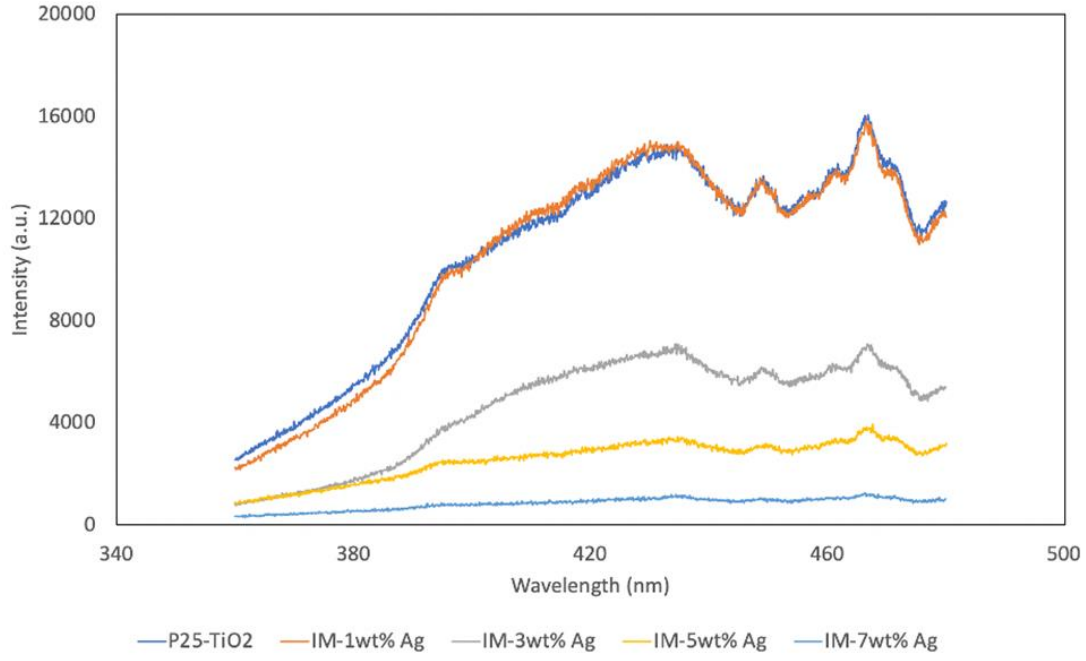

Figure 33: PL spectra of P25 and IM-TiO_2 photocatalysts

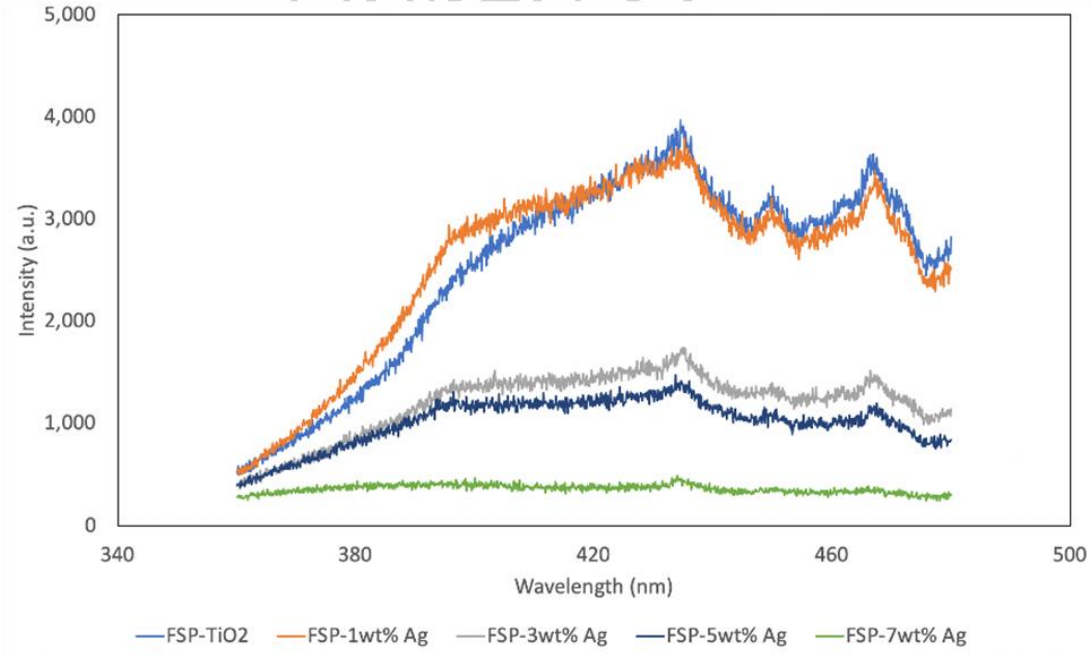

Figure 34: PL spectra of pure TiO_2 and FSP-TiO_2 photocatalysts

5.1.5 Transmission electron microscopy (TEM)

Transmission electron microscopy (TEM) are used to determine the size and morphology of as prepared photocatalysts. TEM images and the size distribution of particles graph of all Ag/TiO_2 photocatalysts are presented in figure 35-38 and figure 39 respectively. TEM images of IM-5wt% Ag/TiO_2 exhibited the nearly spherical shape of TiO_2 and well-dispersed Ag particles with an average particle size around 3.2 nm. Figure 36 shows TEM images of IM-7wt% Ag/TiO_2 photocatalyst. TEM images of IM-7wt% Ag/TiO_2 exhibited the nearly spherical shape of TiO_2 with well-dispersed Ag particles of a size around 2.9 nm. The size of pure TiO_2 from P25 were estimated from TEM image at around 30 nm, which was in good agreement with the value of crystallite size calculated from XRD pattern using the Scherrer equation. Figure 37 shows TEM images of FSP-5wt% Ag/TiO_2 photocatalyst. TEM images of FSP-5wt% Ag/TiO_2 exhibited the nearly spherical shape of TiO_2 and well-dispersed Ag particles of a size around 3.2 nm. Figure 38 shows TEM images of FSP-7wt% Ag/TiO_2 photocatalyst. TEM images of FSP-7wt% Ag/TiO2 exhibited the nearly spherical shape of TiO_2 and well-dispersed Ag particles of a size around 2.97 nm. The size of pure TiO_2 from FSP-TiO_2 were estimated from TEM image is similarly which confirms the value of crystallite size calculated from XRD pattern using the Scherrer equation.

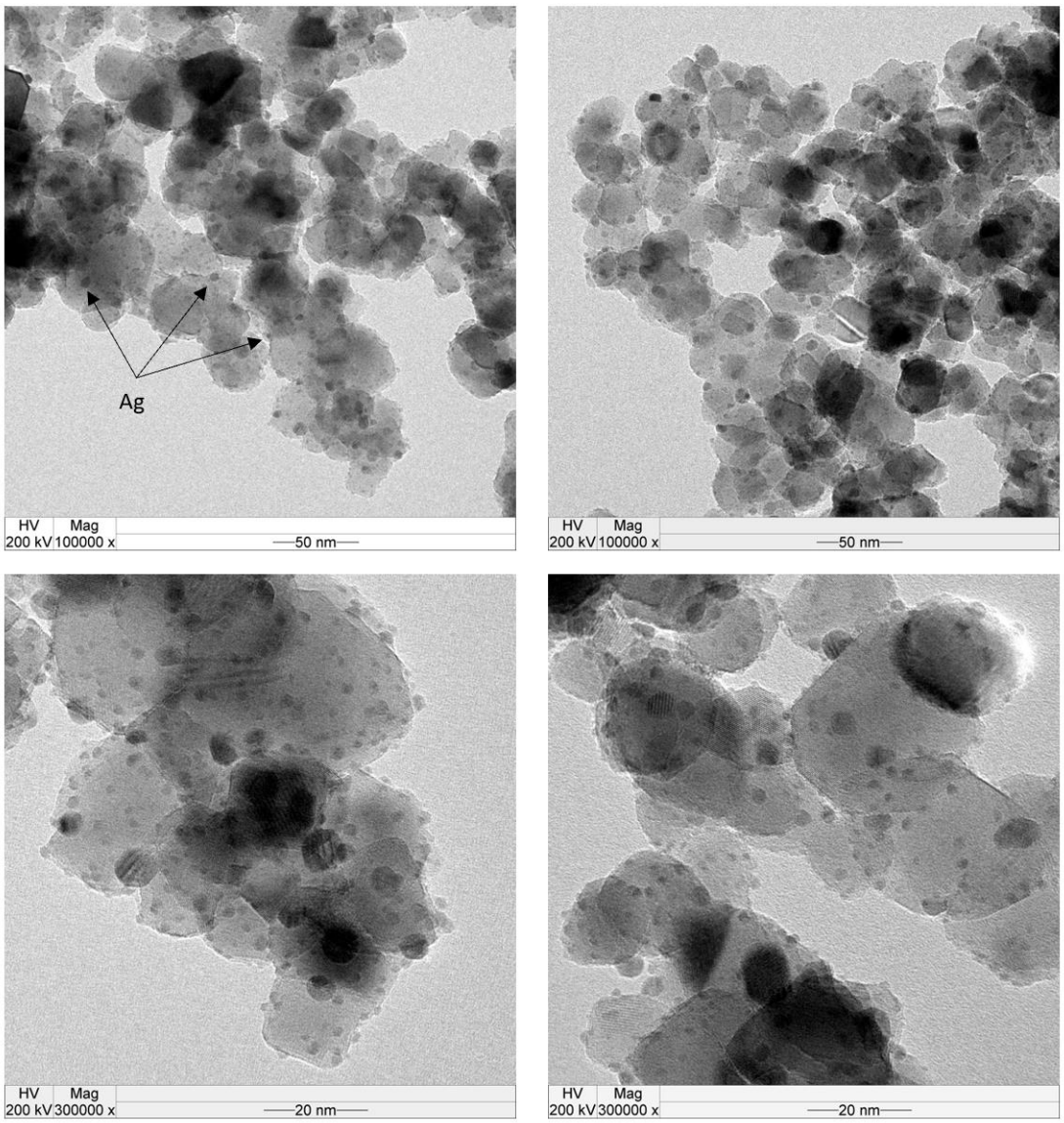

Figure 35: TEM micrographs of IM-5wt% Ag/TiO_2

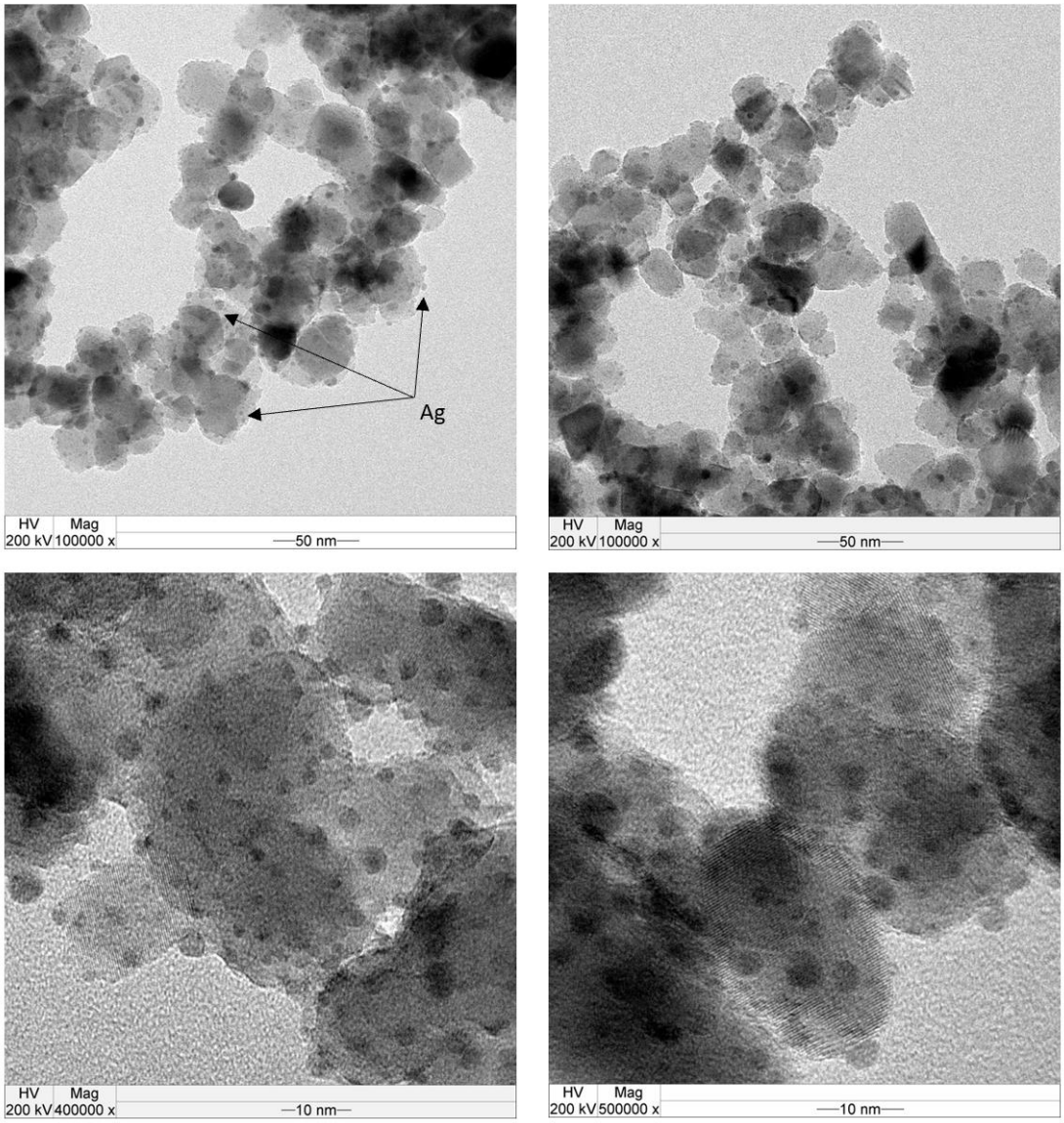

Figure 36: TEM micrographs of IM-7wt% Ag/TiO_2

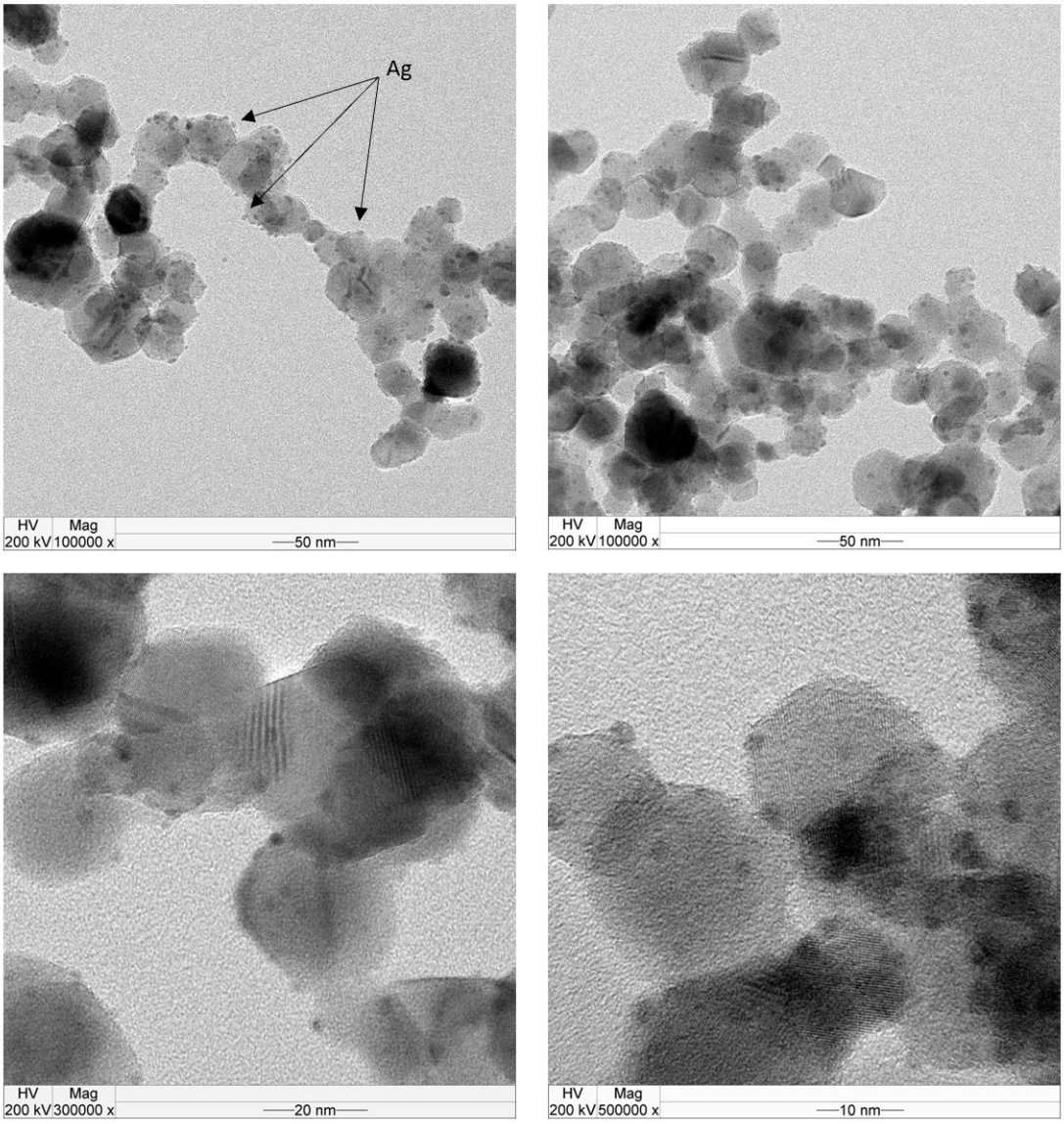

Figure 37: TEM micrographs of FSP-5wt% Ag/TiO_2

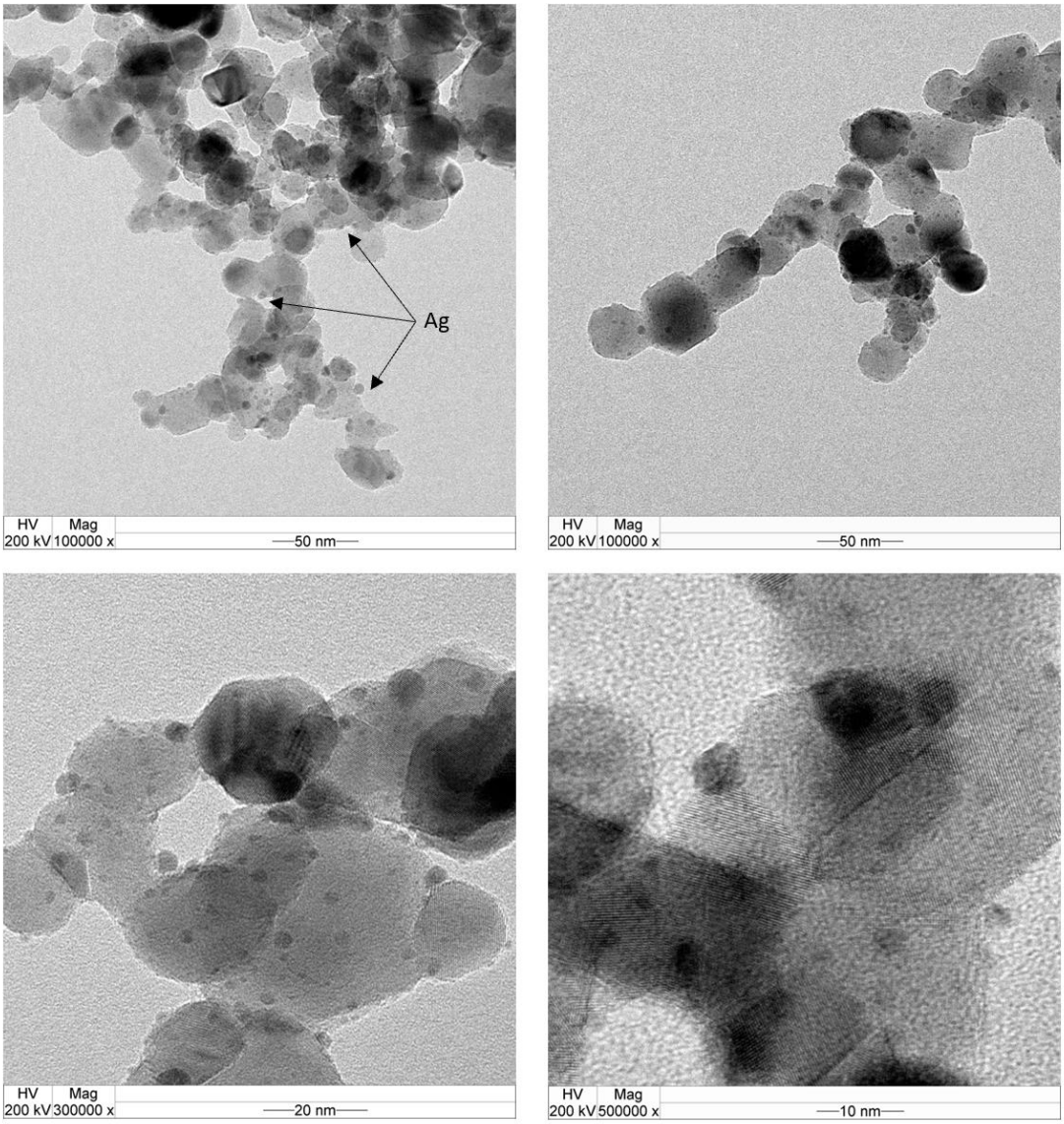

Figure 38: TEM micrographs of FSP-7wt% Ag/TiO_2

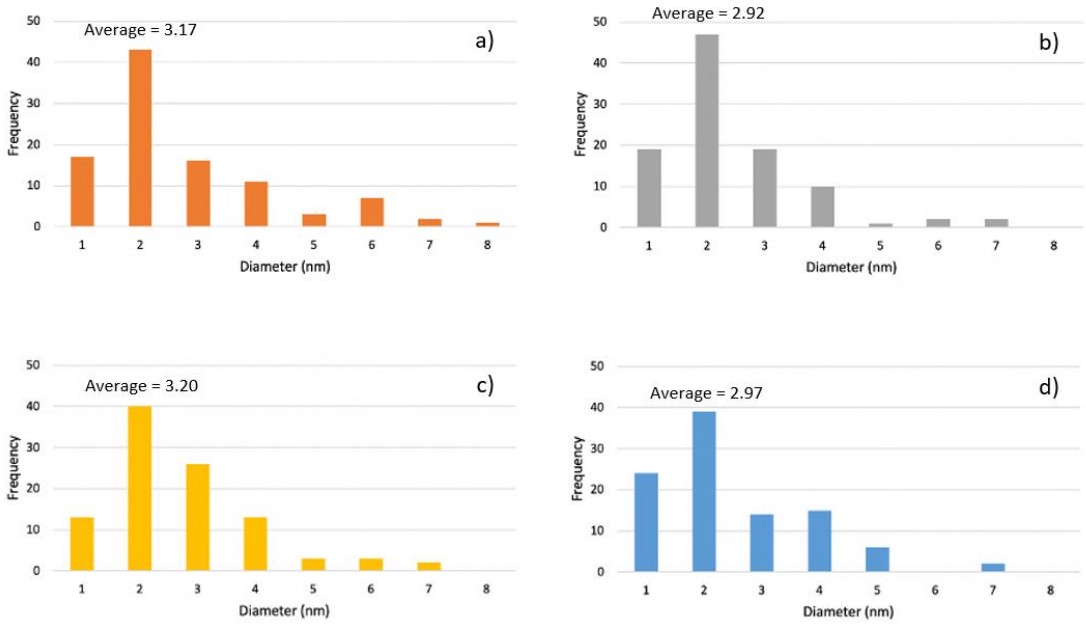

Figure 39: The particle size distribution curve of a) IM-5wt% Ag/TiO_2, b) IM-7wt% Ag/TiO_2, c) FSP-5wt% Ag/TiO_2 and d) FSP-7wt% Ag/TiO_2

5.1.6 X-ray photoelectron spectroscopy (XPS)

X-ray photoelectron spectroscopy (XPS) are used to determines the surface properties of P25, IM-5wt% Ag/TiO_2, FSP-TiO_2, FSP-5wt% Ag/TiO_2 and FSP-7wt% Ag/TiO_2. The XPS spectra of Ti 2p, O 1s and Ag 3d and the element compositions (%) are shown in figure 40-52 and the percentage of photocatalysts table 7-8. The binding energy of Ti $2p_{1/2}$ and Ti $2p_{3/2}$ were located at about 465 eV and 459 eV respectively. These peaks are according with the valance state of Ti4+ on lattice oxygen [66, 67, 78] and detect Ti^{3+} form on oxygen vacancy [79]. The Ti^{3+}/Ti^{4+} ratio of FSP-made catalysts was more than P25 and FSP-made catalysts which according to amount of oxygen vacancies. The binding energy of O 1s were located at about 530.7 eV and 532 eV respectively. The valance state of O is lattice oxide ions in TiO_2 and the hydroxyl groups (R-OH) on the TiO_2 surface such as C-OH bond, Ti-OH bond and C=O bond were excited at 532.3 eV, 531.2 eV and 530.2 eV respectively [80]. The binding energy of oxygen bonded with silver (Ag-O) and TiO_2 crystal lattice (Ti-O-Ti) were identified about 529.8 eV [79]. The oxygen vacancies of FSP-made catalysts were more than P25 and FSP-made catalysts which lead to increase the defect on surface of photocatalysts. The binding energy of Ag $3d_{5/2}$ and Ag $3d_{3/2}$ were located at about 368.2 eV and 374.3 eV respectively which show in figure 55. The valance state of Ag is Ag^0, Ag^{1+} and Ag^{2+} on lattice oxygen [66, 67, 78] which accord with 368.3 eV, 367.6 eV and 367.05 eV respectively [79]. The silver content in the surface layer of all photocatalysts shows the Ag species in the metallic state [79, 80]. Which confirms the value of crystalline structure from XRD pattern and the morphology from TEM images. The Ti^{3+}/Ti^{4+} ratio and oxygen vacancies (O_V) of used FSP-7wt% Ag/TiO_2 photocatalyst were decreased due to the use of recycle to check its stability. Which shows in figure 53-54 and table 10.

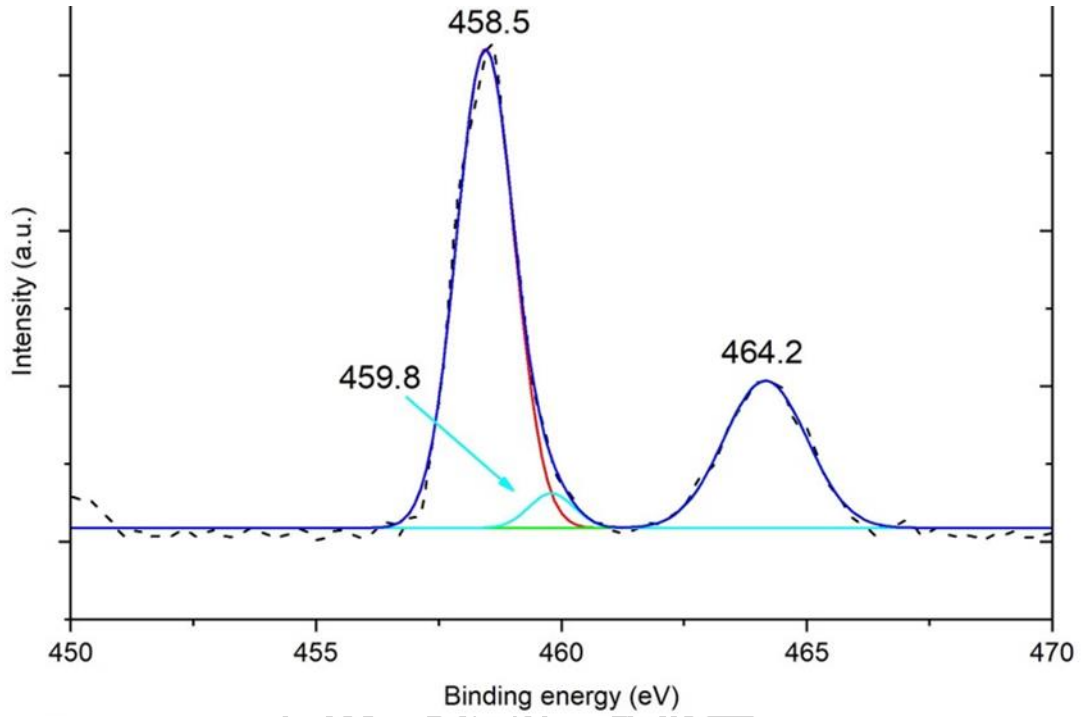

Figure 40: XPS spectra of Ti 2p of P25

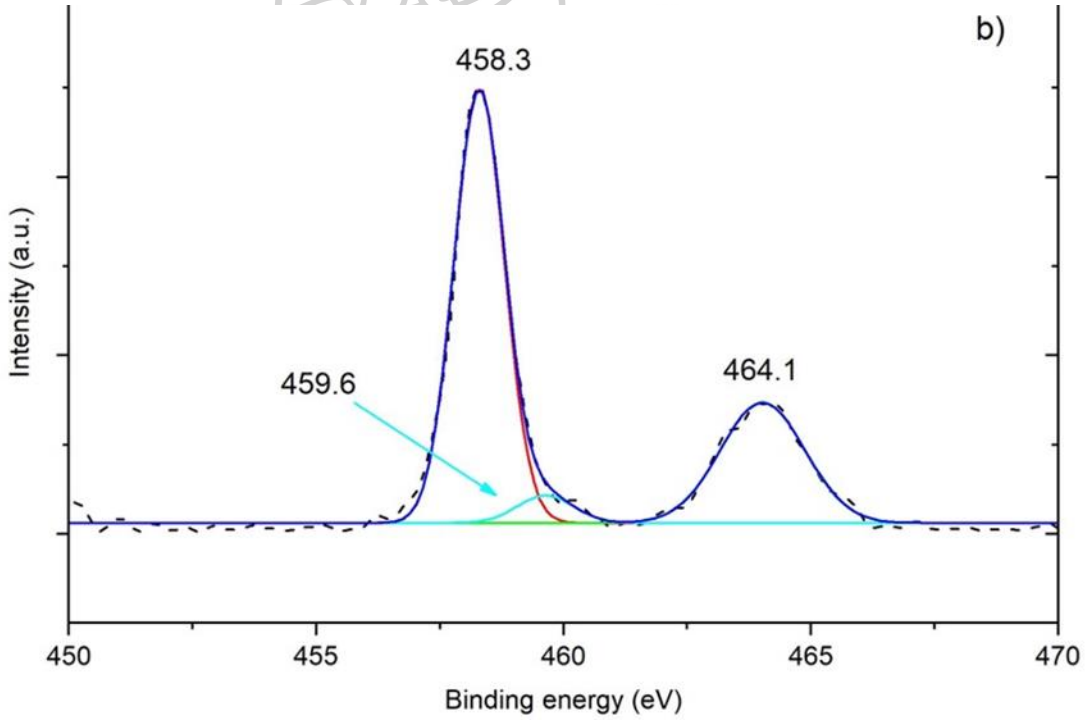

Figure 41: XPS spectra of Ti 2p of IM-5wt% Ag/TiO_2

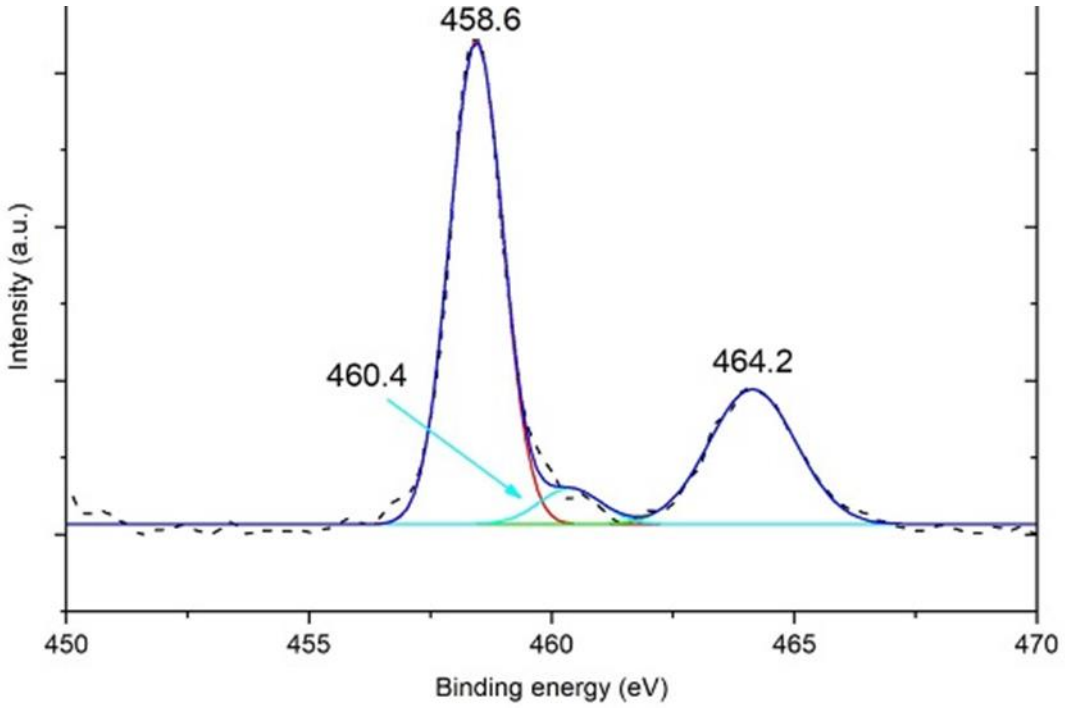

Figure 42: XPS spectra of Ti 2p of FSP-TiO_2

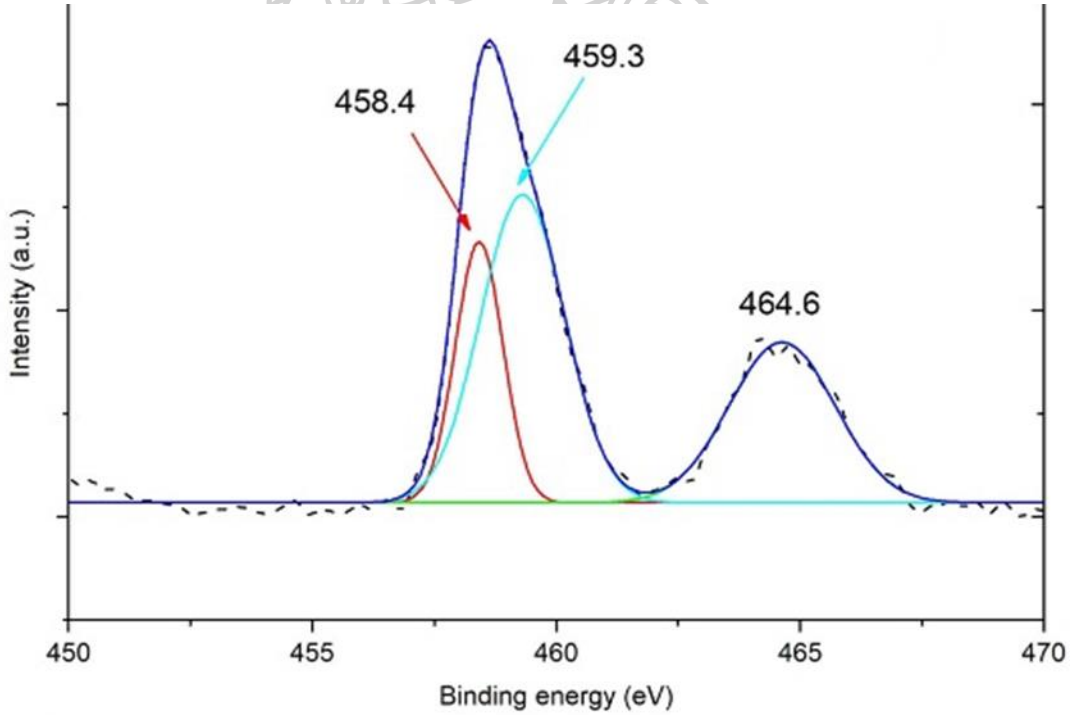

Figure 43: XPS spectra of Ti 2p of FSP-5wt% Ag/TiO_2

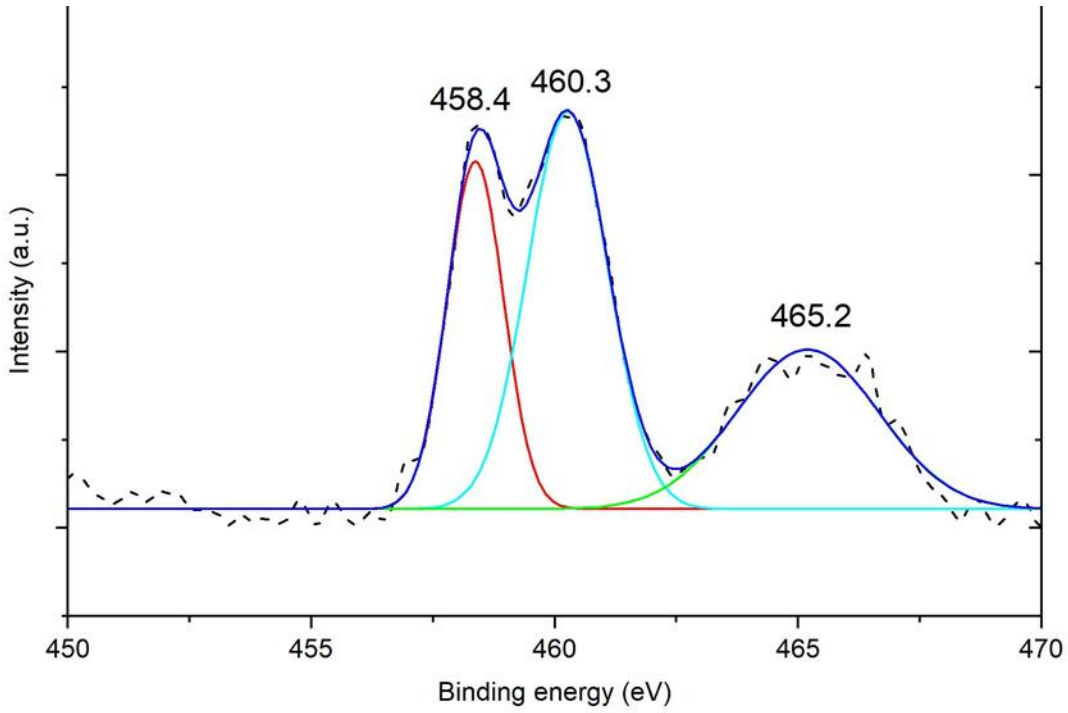

Figure 44: XPS spectra of Ti 2p of FSP-7wt% Ag/TiO_2

Table 7: Calculation the percentage of peak area of titania for TiO_2

Samples	Binding energy (eV)	Peak	Peak area	Ratio of peak area Ti^{3+}/ Ti^{4+}
P25	458.5	Ti^{4+} ($2p_{3/2}$)	4543.99	0.053
	459.8	Ti^{3+} ($2p_{3/2}$)	255.54	
IM-5wt% Ag/TiO_2	458.3	Ti^{4+} ($2p_{3/2}$)	3092.65	0.066
	459.6	Ti^{3+} ($2p_{3/2}$)	219.74	
FSP-TiO_2	458.6	Ti^{4+} ($2p_{3/2}$)	4373.31	0.079
	460.4	Ti^{3+} ($2p_{3/2}$)	374.32	
FSP-5wt% Ag/TiO_2	464.6	Ti^{4+} ($2p_{1/2}$)	3655.75	0.47
	459.3	Ti^{3+} ($2p_{3/2}$)	3225.39	
FSP-7wt% Ag/TiO_2	465.2	Ti^{4+} ($2p_{1/2}$)	1662.47	0.59
	460.3	Ti^{3+} ($2p_{3/2}$)	2348.37	

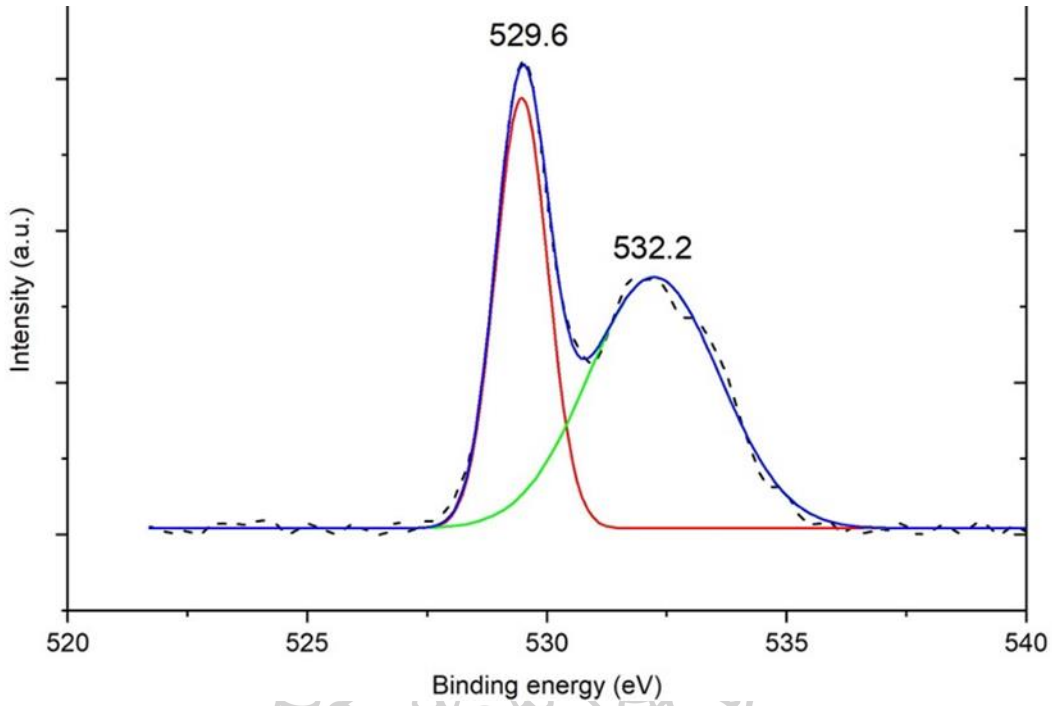

Figure 45: XPS spectra of O 1s of P25

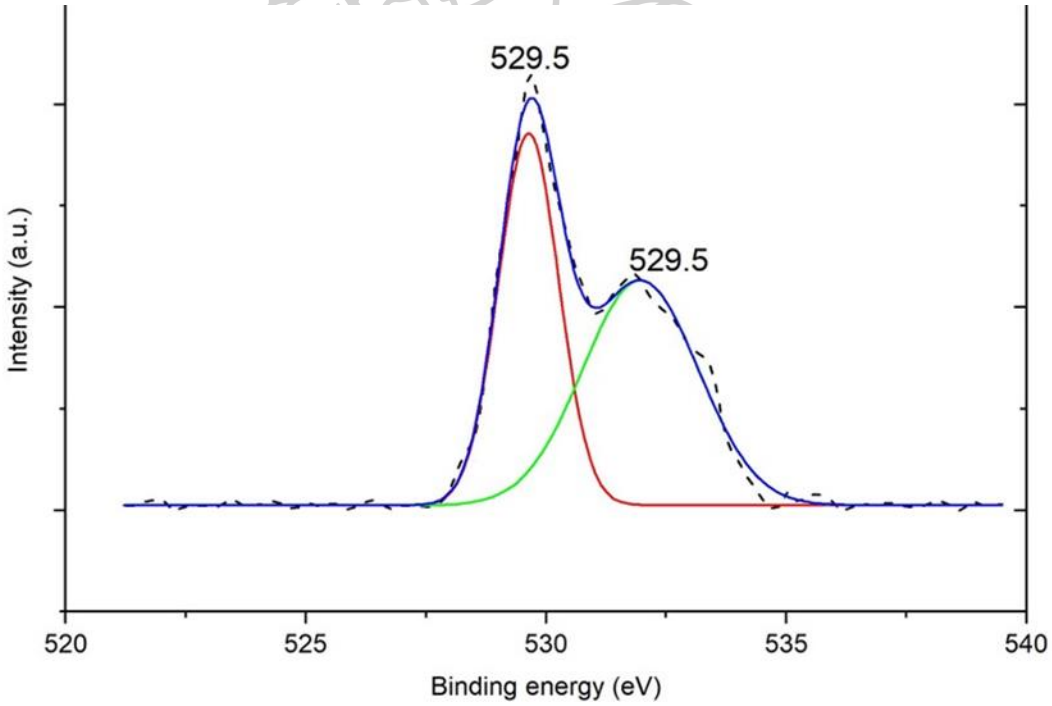

Figure 46: XPS spectra of O 1s of IM-5wt% Ag/TiO_2

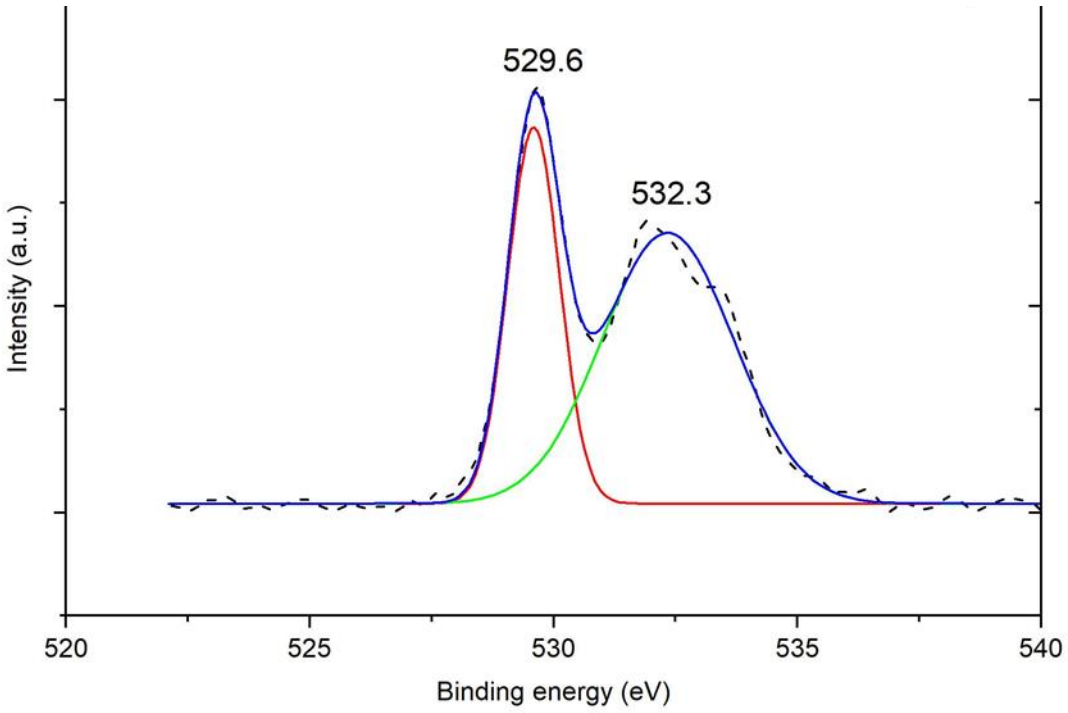

Figure 47: XPS spectra of O 1s of FSP-TiO_2

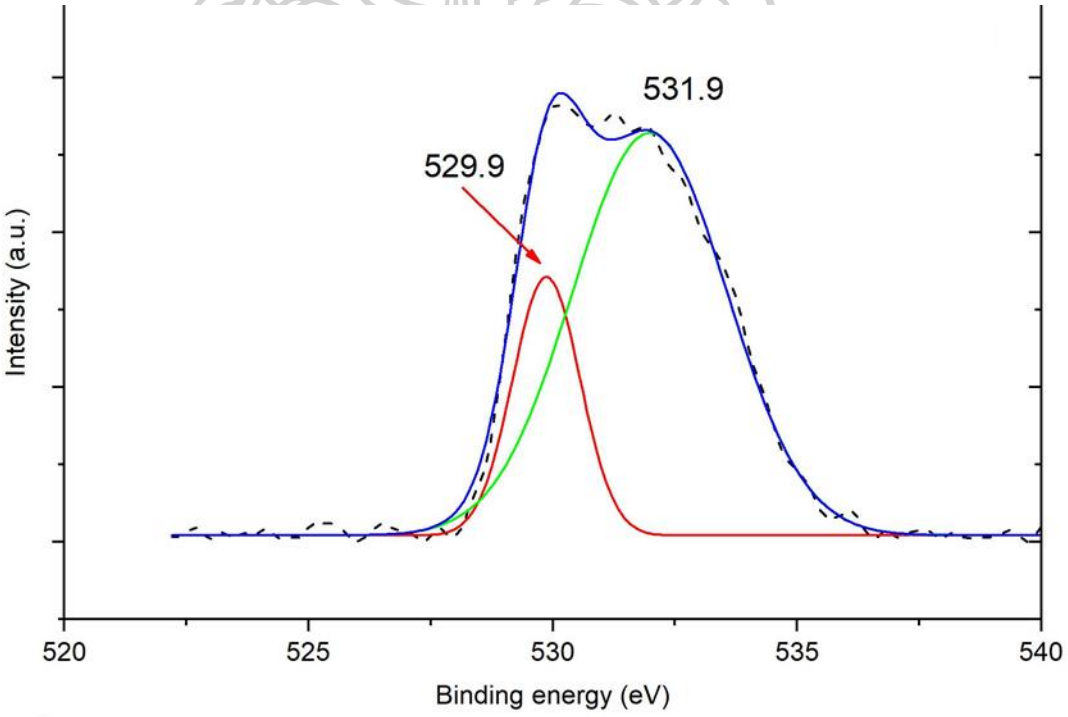

Figure 48: XPS spectra of O 1s of FSP-5wt% Ag/TiO_2

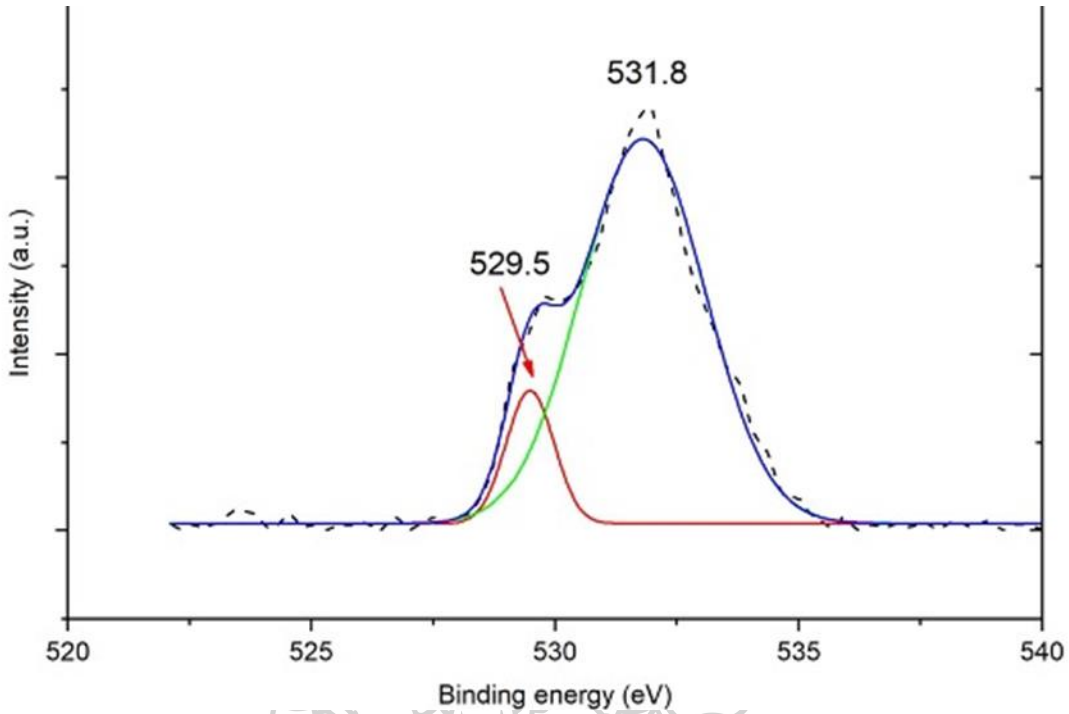

Figure 49: XPS spectra of O 1s of FSP-7wt% Ag/TiO_2

Table 8: Calculation the percentage of peak area of oxygen for TiO_2

Samples	Binding energy (eV)	Peak	Peak area	%Peak area
P25	532.0	Oxygen vacancies (O_V)	6668.85	46.29
	529.6	Oxygen lattices (O_L)	5747.65	53.71
IM-5wt% Ag/TiO_2	531.8	Oxygen vacancies (O_V)	5696.21	59.39
	529.5	Oxygen lattices (O_L)	3895.45	40.61
FSP-TiO_2	532.3	Oxygen vacancies (O_V)	8903.78	64.85
	529.6	Oxygen lattices (O_L)	4826.89	35.15
FSP-5wt% Ag/TiO_2	532.0	Oxygen vacancies (O_V)	10290.93	78.17
	529.9	Oxygen lattices (O_L)	2873.84	21.83
FSP-7wt% Ag/TiO_2	531.8	Oxygen vacancies (O_V)	6951.31	88.24
	529.5	Oxygen lattices (O_L)	926.82	11.76

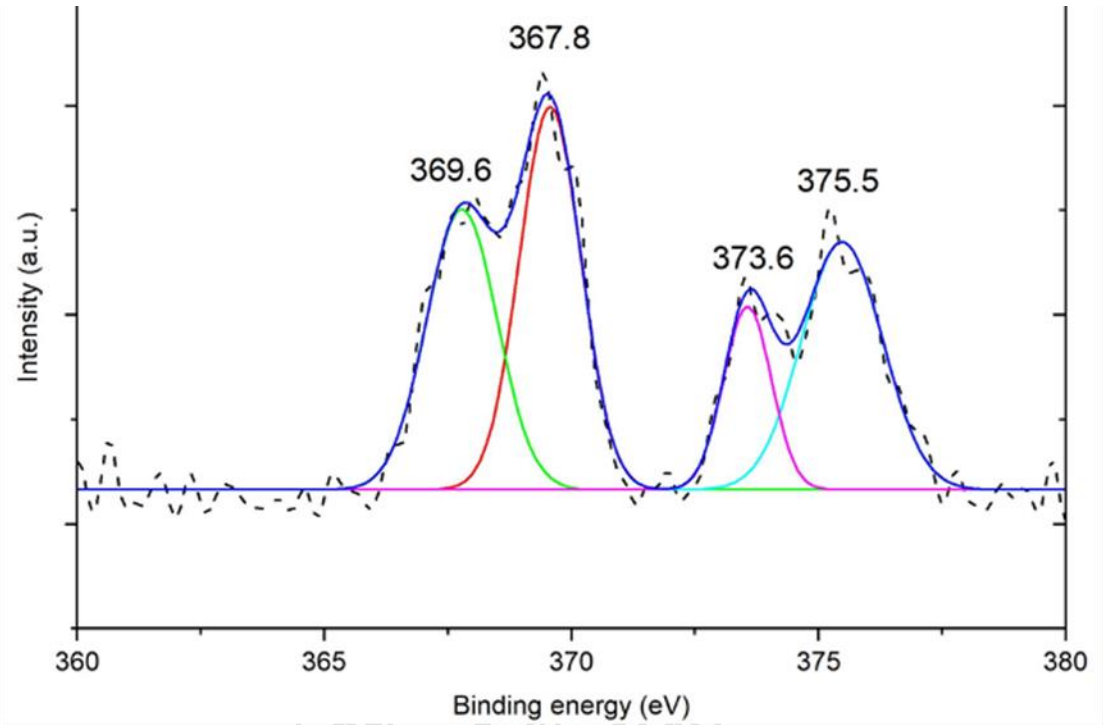

Figure 50: XPS spectra of Ag 3d of IM-5wt% Ag/TiO_2

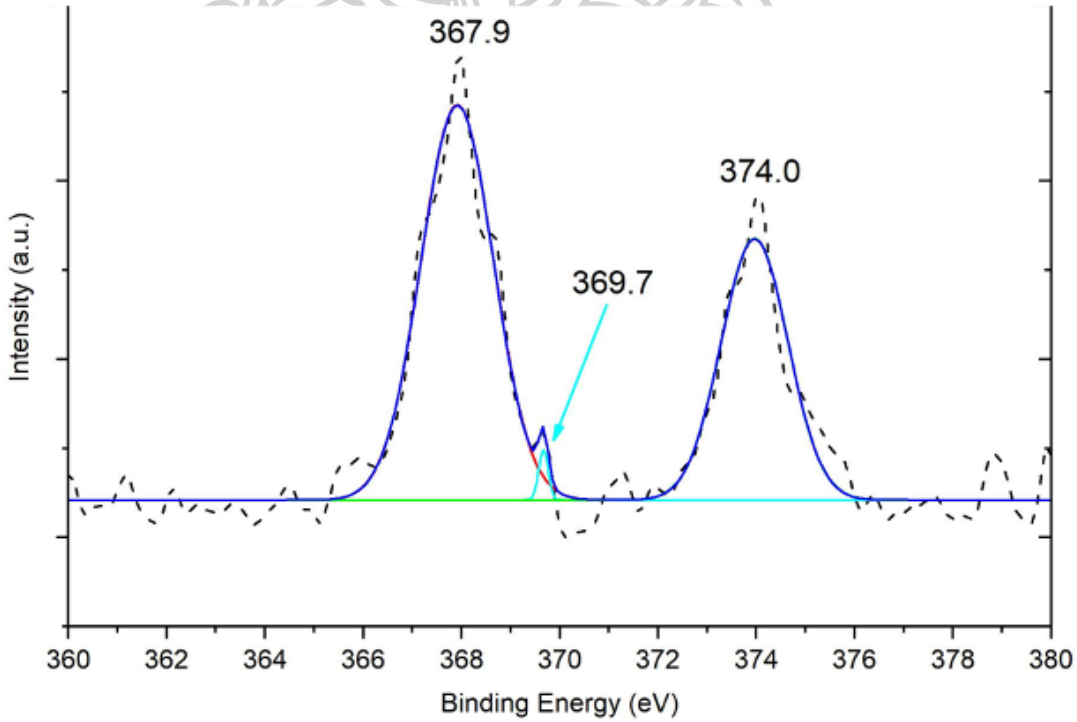

Figure 51: XPS spectra of Ag 3d of FSP-5wt% Ag/TiO_2

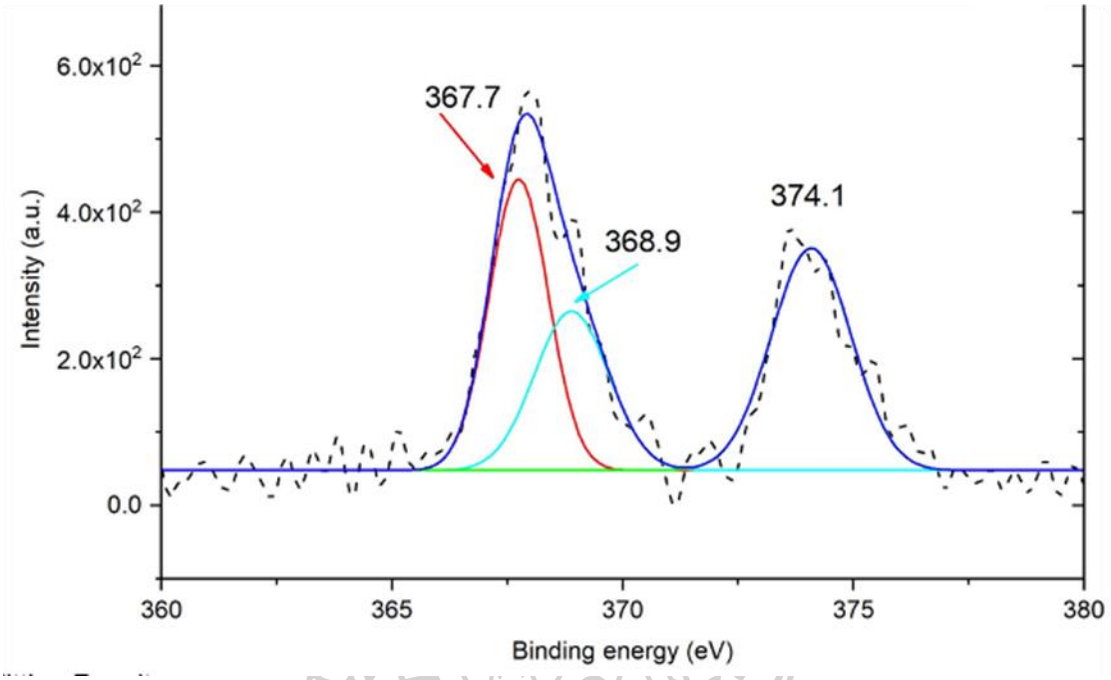

Figure 52: XPS spectra of Ag 3d of FSP-7wt% Ag/TiO_2

Table 9: Calculation the percentage of peak area of silver for TiO_2

Samples	Binding energy (eV)	Peak	Peak area	%Peak area
IM-5wt%	369.6	Ag^{1+} + Ag^{2+} ($3d_{5/2}$)	572.50	53.97
Ag/TiO_2	373.6	Ag^{0} ($3d_{3/2}$)	488.21	46.03
FSP-5wt%	367.9	Ag^{1+} + Ag^{2+} ($3d_{5/2}$)	817.67	62.11
Ag/TiO_2	374.0	Ag^{0} ($3d_{3/2}$)	498.72	37.89
FSP-7wt%	367.7	Ag^{1+} + Ag^{2+} ($3d_{5/2}$)	636.66	49.15
Ag/TiO_2	374.1	Ag^{0} ($3d_{3/2}$)	658.70	50.85

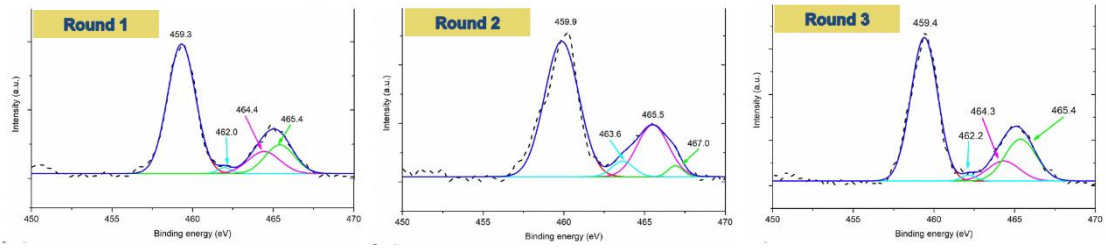

Figure 53: XPS spectra of Ti 2p of used FSP-7wt% Ag/TiO_2

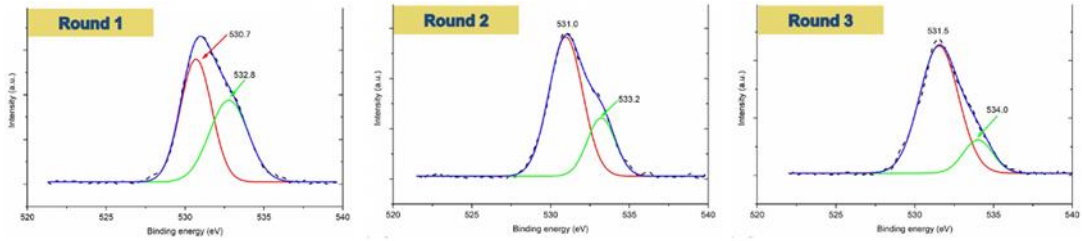

Figure 54: XPS spectra of O 1s of used FSP-7wt% Ag/TiO_2

Table 10: Calculation the percentage of peak area of used FSP-7wt% Ag/TiO_2

Round	Ratio of peak area Ti^{3+}/ Ti^{4+}	Ratio of peak area O_V/O_L
Fresh	0.59	0.88
Used 1st round	0.26	0.45
Used 2nd round	0.25	0.25
Used 3rd round	0.19	0.17

5.2 Photocatalytic activity

The photocatalytic activity of pure TiO_2 and all the Ag/TiO_2 photocatalysts are evaluated by CO_2 reduction of photocatalyst in water at ambient temperature under UVC irradiation. From our test results, methane (CH_4) is a main product which obtained from all photocatalysts and low amounts of hydrogen (H_2) and carbon monoxide (CO) were also detected. The other products such as formic acid, formaldehyde, ethane and ethylene were undetected [17, 33]. Figure 56 shows the graph between the production yield of CH_4 from P25 and all IM-Ag/TiO_2 photocatalysts after 3 h reaction. It can be seen that IM-5wt% Ag/TiO_2 has a greatest effect on the photocatalytic activity among P25 and IM-made photocatalysts. Addition of Ag also promoted the catalytic activity of the photocatalysts. IM-5wt% Ag/TiO_2 shows the best photocatalytic activity. Moreover, the investigation was exhibited the increasing reaction rate with the increasing of Ag content. IM-7wt% Ag/TiO_2 exhibited the lower photocatalytic activity when that was compared with IM-5wt% Ag/TiO_2. The cause of IM-7wt% Ag/TiO_2 is due to amount of Ag doped on TiO_2 which is unsuitable. That may exhibit the electron-hole (e^-/h^+) recombination centers. This phenomenon negatively affects the photocatalytic efficiency. Therefore, the suitable Ag doped on TiO_2 can improve the photocatalytic activity of TiO_2 support. The yield CH_4 of IM-5wt% Ag/TiO_2 photocatalyst exhibits the yield CH_4 higher than P25 and IM-made photocatalysts which is 0.75 umol/gcat.h in figure 56. Figure 58 shows the graph production of the yield CH_4 from FSP-TiO_2 and FSP-Ag/TiO_2 photocatalysts after 3 h reaction. FSP-7wt% Ag/TiO_2 has the best activity from FSP-made photocatalysts. The FSP-TiO_2 has a badly activity on the yield CH_4 production compared with FSP-Ag/TiO_2 photocatalysts. FSP-7wt% Ag/TiO_2 shows the best photocatalytic activity between these. Therefore, this experiment exhibited the increasing reaction rate when increasing Ag content was doped on TiO_2 support. Figure 55-58 showed the best yield CH_4 of FSP-7wt% Ag/TiO_2 photocatalyst higher than FSP-made photocatalysts and all photocatalysts in figure which is 2.22 umol/gcat.h. Figure 60 shows the graph production yield of CH_4 from FSP-7wt% Ag/TiO_2 in varied NaOH concentration. It can be shown that FSP-7wt% Ag/TiO_2 in DI water has a great effect on the photocatalytic activity which was compared with

0.1M NaOH, 0.2M NaOH and 0.3M NaOH. Figure 61-62 shows the stability of FSP-7wt% Ag/TiO_2. The yield CH_4 of first round is 2.22 umol/gcat.h after that second round and third round are decreased to 1.85 umol/gcat.h and 1.36 umol/gcat.h respectively as. The cause of this result was shown in figure 53-54 and table 10.

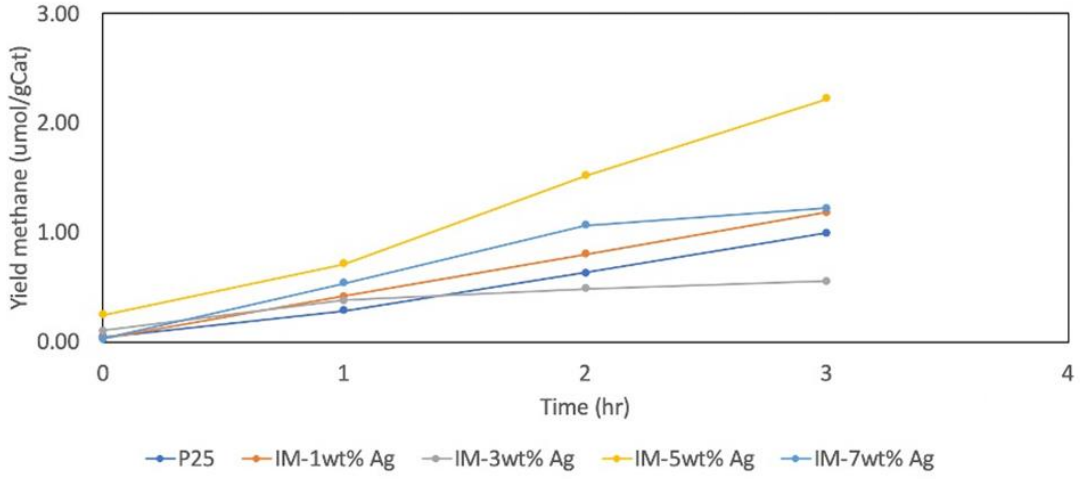

Figure 55: Graph between yield methane (CH_4) and time over the IM-Ag/TiO_2 photocatalysts

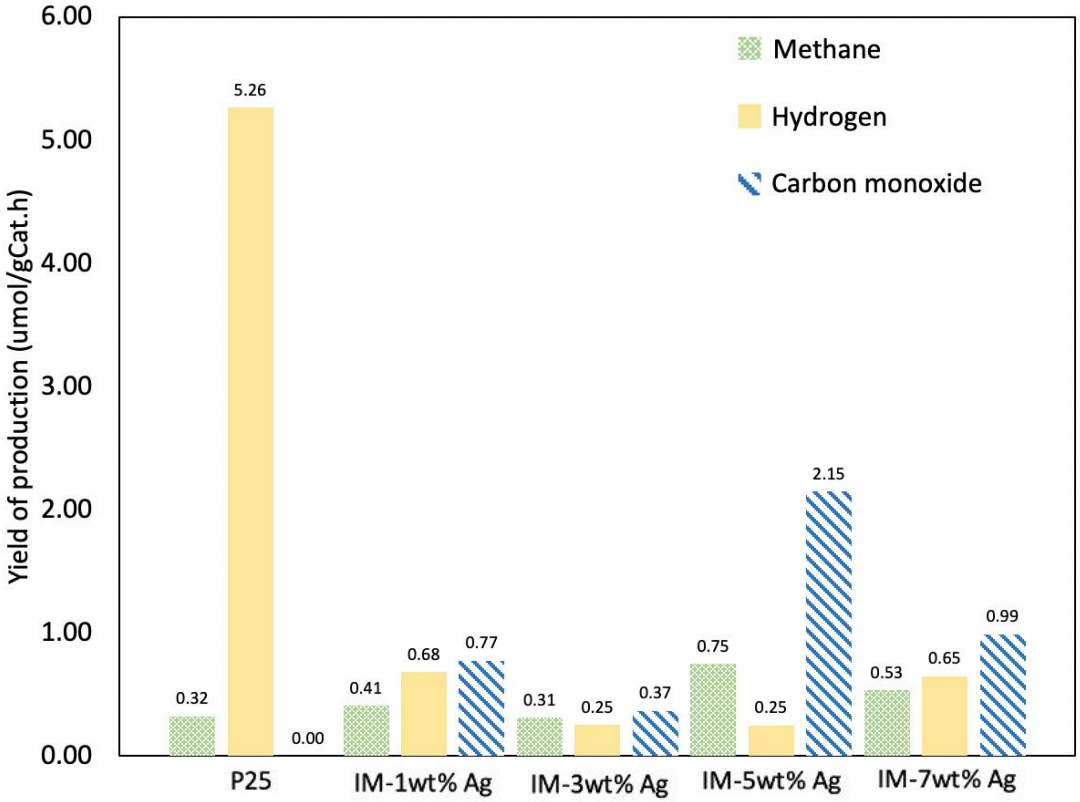

Figure 56: Yield of production over the IM-Ag/TiO_2 photocatalysts (after 3 h reaction time)

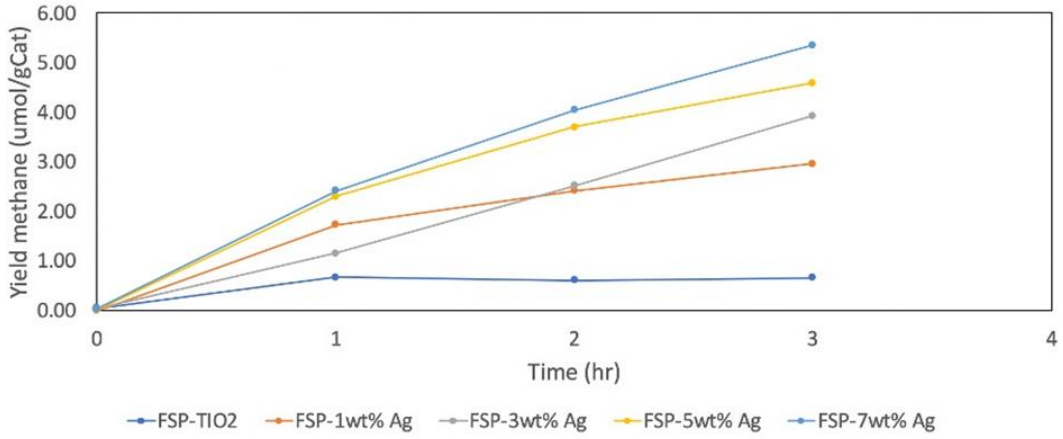

Figure 57: Graph between yield methane (CH_4) and time over the FSP-Ag/TiO_2 photocatalysts

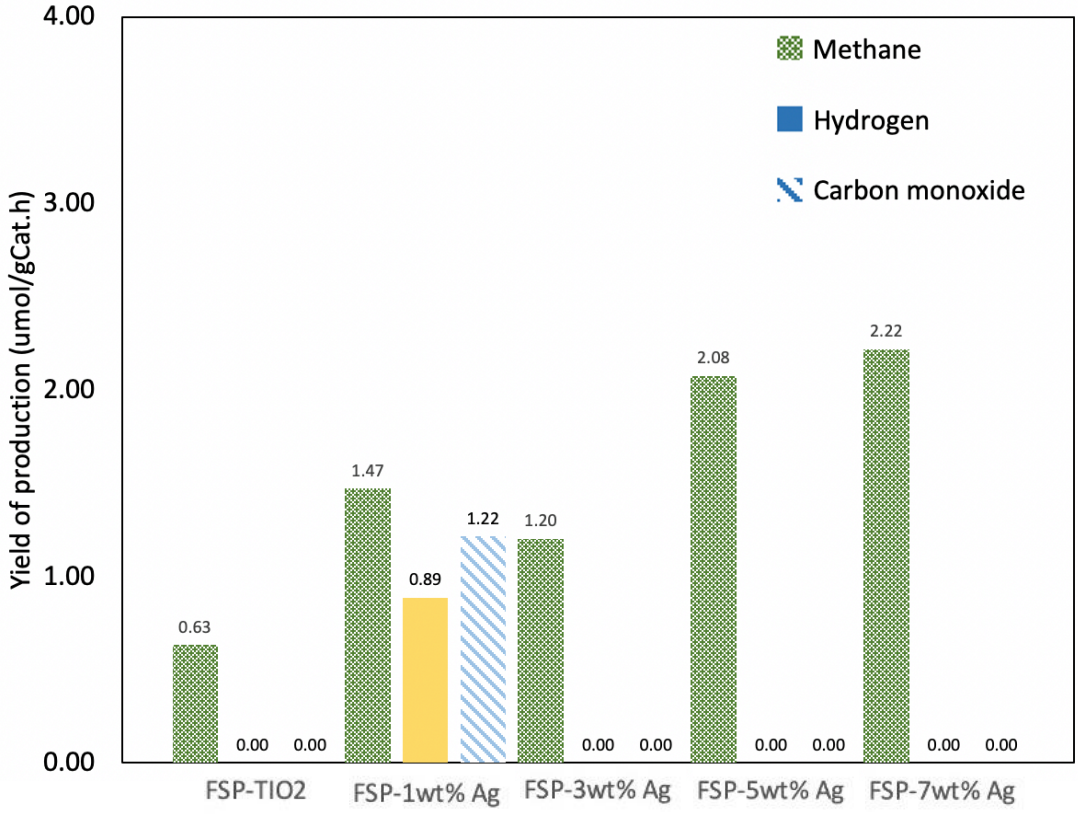

Figure 58: Yield of production over the FSP-Ag/TiO_2 photocatalysts (after 3 h reaction time)

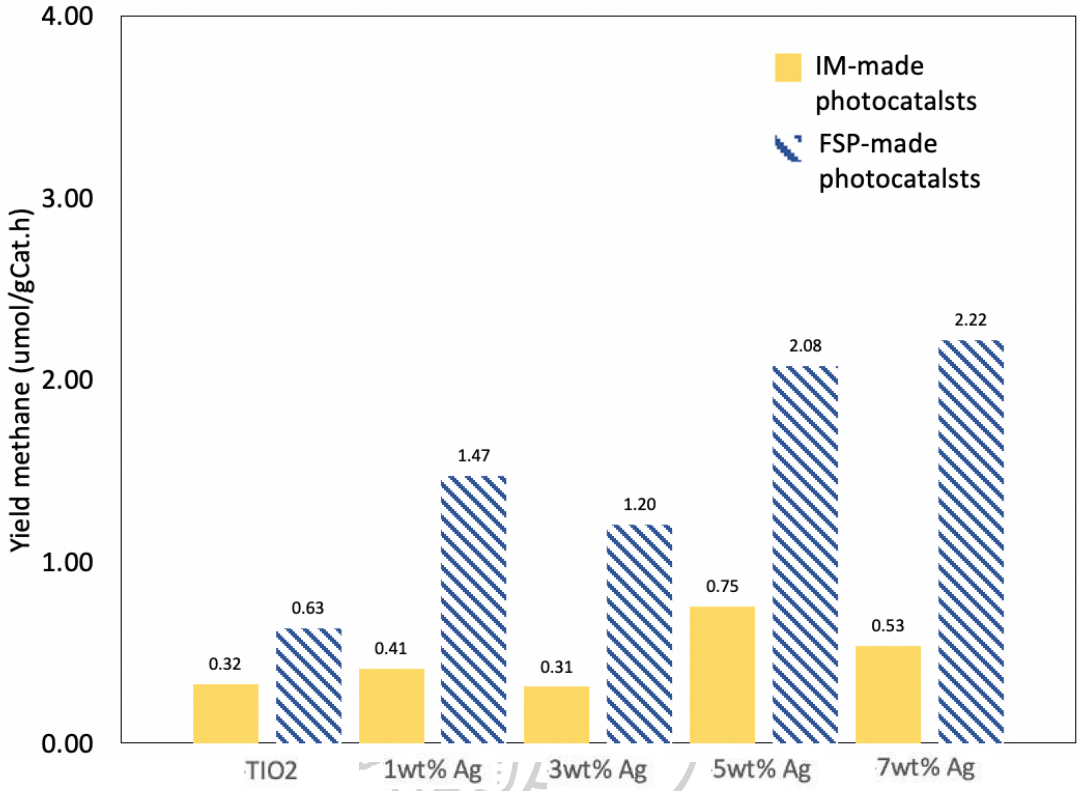

Figure 59: Yield of methane (CH_4) over the Ag-doped TiO_2 photocatalysts (after 3 h reaction time)

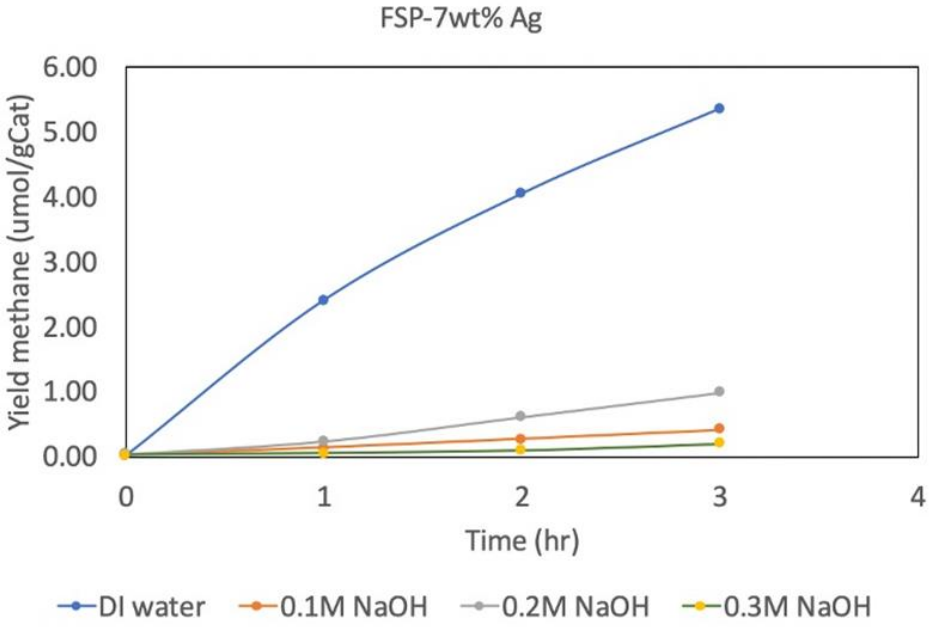

Figure 60: Graph between yield methane (CH_4) and time in varied NaOH concentration of FSP-7wt%

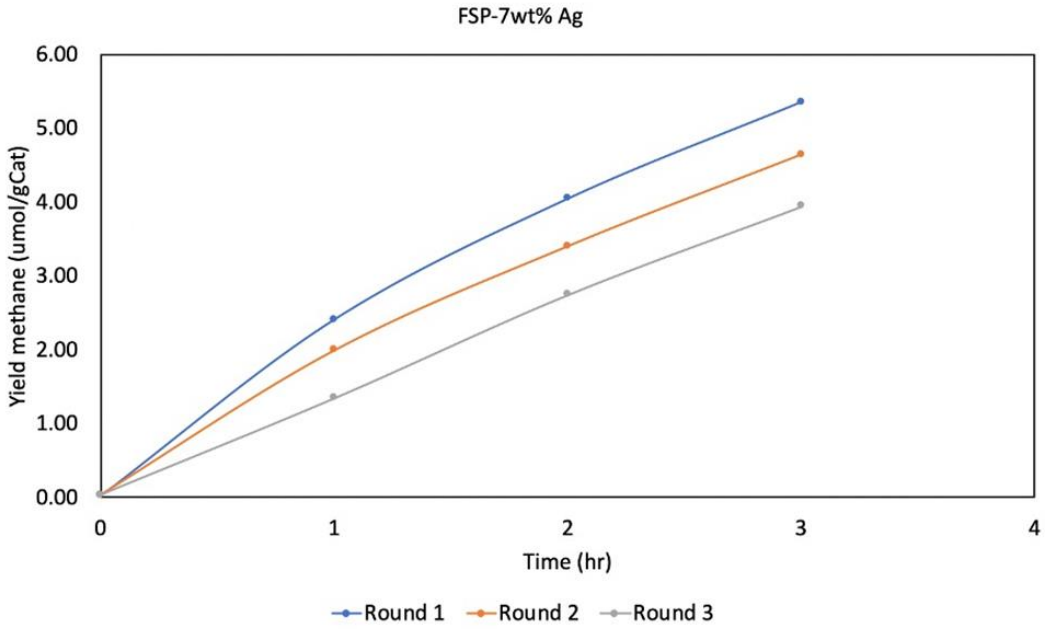

Figure 61: Graph between yield methane (CH_4) and time of FSP-7wt% Ag/TiO_2

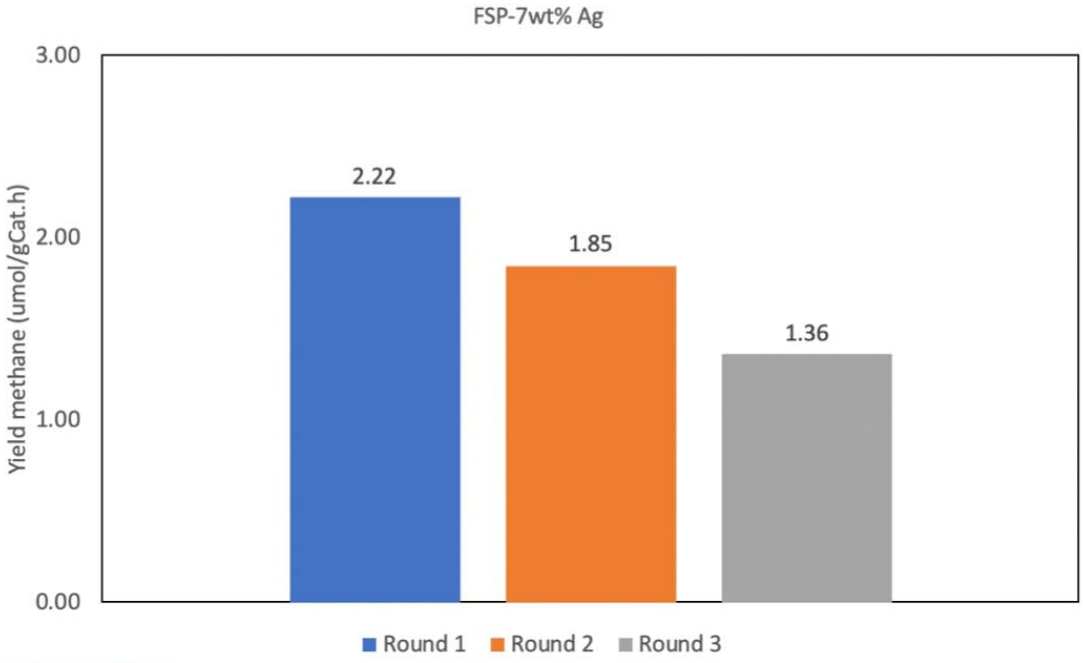

Figure 62: Stability of FSP-7wt% Ag/TiO_2

CHAPTER VI

CONCLUSION

6.1 Conclusions

Ag/TiO_2 photocatalysts with various amounts of silver (Ag) doping have successfully prepared by using flame spray pyrolysis (FSP) and dry impregnation (IM) method. The XRD pattern of IM-Ag/TiO_2 and FSP-Ag/TiO_2 photocatalysts exhibited only the peaks according to rutile and anatase TiO_2 because of well-dispersed Ag particles on TiO_2 supports, on the other hand, only FSP-7wt% Ag/TiO_2 photocatalysts showed the presence of Ag metal phase. From XPS result, the Ti^{3+} and oxygen vacancies of FSP-made photocatalysts was higher than IM-made photocatalysts. The PL spectra confirm the electron-hole recombination rate of all photocatalysts decreased as the increased of Ag doping. From PL results, the recombination rate FSP-made photocatalysts were much less than IM-made photocatalysts. The UV-Vis spectra also revealed that the increased Ag doping content leaded to improve the ability of absorption at visible light region. The TEM images of IM-made and FSP-made photocatalysts showed the well-dispersion Ag metal on TiO_2 support. From the reaction test, the photocatalytic activity of FSP-made catalysts was higher compare with IM-made one. The CH_4 yield of FSP-7wt% Ag/TiO_2 is highest among all photocatalysts at 2.22 umol/gCat.h. The higher catalytic activity would be due to the higher of Ti^{3+} of FSP-made catalysts. Addition of Ag also promoted the photocatalytic activity due to the Ag can act as electron trap sites, which decreased the electron-hole recombination.

6.2 Recommendation

6.2.1 Investigate the effect of other condition such as light source and other pH of solution

6.2.2 Modify or design a photoreactor that lead to highly photocatalytic reaction

APPENDIX A

CALCULATION FOR CATALYST PREPARATION

Table 11: Chemical properties of the catalyst precursor

Chemicals	Molecular weight (g/mole)	Formula	Molecular weight of precursor (g/mole)	Purity (%)
Titanium (IV) isopropoxide	79.87	$Ti\{(OCH(CH_3))_2\}_4$	284.22	97
Silver (I) nitrate	107.87	$Ag(NO_3)$	169.87	99.5
Titanium (II) oxide	79.87	TiO_2	79.88	>99

Calculation of mixed metal oxide support prepared by impregnation method

For example:

The calculation for the preparation of Ag doped on TiO_2, Titanium (II) oxide with silver (I) nitrate as Ag precursor

Base on 100g of catalyst used, the composition of the catalyst will be as follows:

Ag = 1g and Support = 99g

For 2 g of support Ag required = 2 x (1/99) = 0.02 g

thus, Ag 0.02g was prepared from **silver (I) nitrate**.

$$\text{Ag precursor required} = \frac{0.02\ \text{g Ag}}{107.87\ \text{g/mole Ag}} \frac{\mathbf{169.87\ precursor\ Ag}}{\mathbf{1\ mole\ Ag}} \times \frac{100}{99.8} = 0.03\ \text{g}$$

Calculation of mixed metal oxide support prepared by flame spray pyrolysis

For example:

The calculation for the preparation of Ag doped on TiO_2, Titanium (IV) isopropoxide and silver (I) nitrate were used as Ag precursor and then diluted with butanol to a 0.5M solution.

The composition of the catalyst will be as follows:

Ag = 1g and TiO_2 = 99g

Conversion to mole fraction Ag $= \frac{1\ g}{107.87\ g/mole} = 9.27 \times 10^{-3}$ mole Ag

$TiO_2 = \frac{99\ g}{79.87\ g/mole} = 1.24$ mol TiO_2

$\therefore$ Total mole fraction = $(9.27 \times 10^{-3}) + 1.24 = 1.24927$ mole

Basis on 500ml of liquid precursor with 0.5M

$$Ag = \frac{\mathbf{9.27 \times 10^{-3}\ mole\ Ag}}{\mathbf{1.24927\ mole}} \times 500ml \times \frac{0.5\ mole}{1000\ ml} = 0.001855 \text{ mole Ag}$$

$$TiO_2 = \frac{\mathbf{1.24\ mole\ TiO_2}}{\mathbf{1.24927\ mole}} \times 500ml \times \frac{0.5\ mole}{1000\ ml} = 0.2481 \text{ mole } TiO_2$$

Calculation of usage chemical precursor

$$\text{Ag precursor} = 0.001855 \text{ mole Ag} \times \frac{\mathbf{169.87\ precursor\ Ag}}{\mathbf{1\ mole\ Ag}} \times \frac{100}{99.8} = 0.316\ g$$

$$TiO_2 \text{ precursor} = 0.2481 \text{ mole } TiO_2 \times \frac{\mathbf{1\ ml}}{\mathbf{0.96\ g/cm^3}} \times \frac{100}{97} = 75.72\ ml$$

APPENDIX B

CALCULATION OF THE CRYSTALLITE SIZE

Calculation of the crystallite size by Debye-Scherrer's equation

The crystallite size was calculated from the half-height width of the diffraction peak of XRD pattern using the Debye-Scherrer's equation.

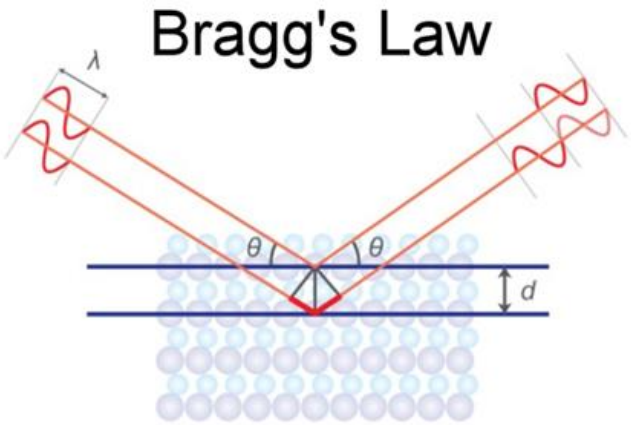

Figure 63: Derivation of Bragg's law of x-ray diffraction

Bragg's law of x-ray diffraction is $d = \frac{n\lambda}{2\sin\theta}$

And Scherrer's equation is $D = \frac{K\lambda}{\beta\cos\theta}$

when D = Crystallite size, Å

K = Crystallite-shape factor = 0.9

λ = X-ray wavelength, 1.5418 Å for Cu$K\alpha$

θ = Observes peak angle, degree

β = X-ray diffraction broadening, radian

The pure width of powder diffraction free from all broadening owing to the experimental equipment was indicated by X-ray diffraction broadening (β). A standard sample to observe the influential broadening was indicated by α-alumina when a crystallite size is larger than 2000Å. Therefore, X-ray diffraction broadening (β) can be calculated by Warren's formula.

Warren's formula is $\beta = \sqrt{B_M^2 - B_S^2}$

when B_M = The measured peak width in radians at half peak height.

B_S = The corresponding width of the standard material.

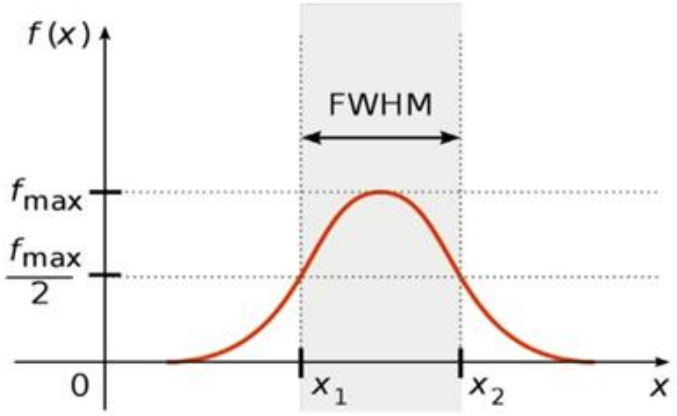

Figure 64: The determining of FWHM value of XRD line broadening

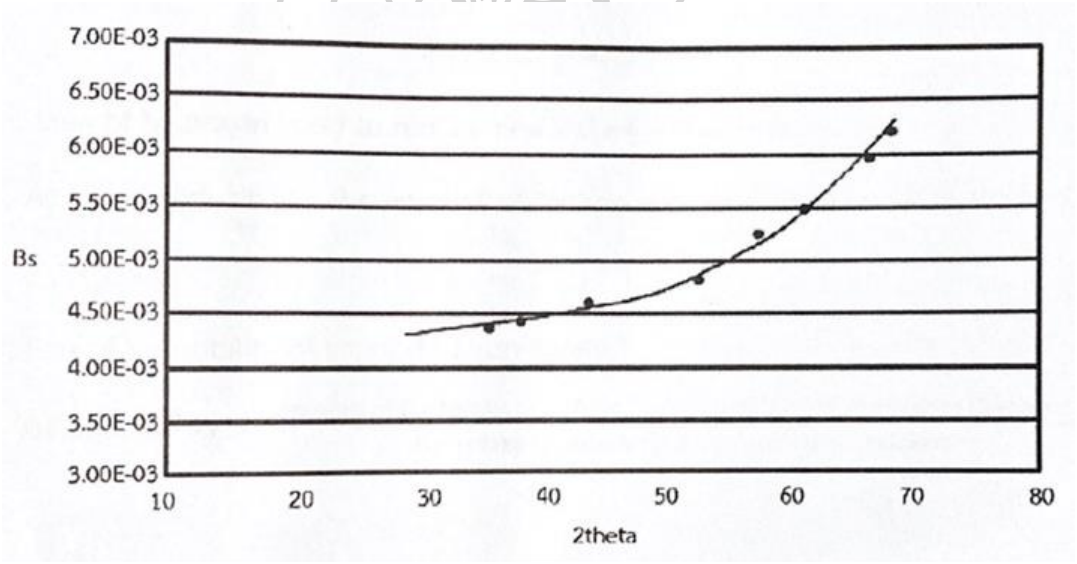

Figure 65: The plot indicating the value of line broadening owing to instrument. The α-alumina is a standard for indicated the data.

For example:

Calculation of the crystallite size of P25

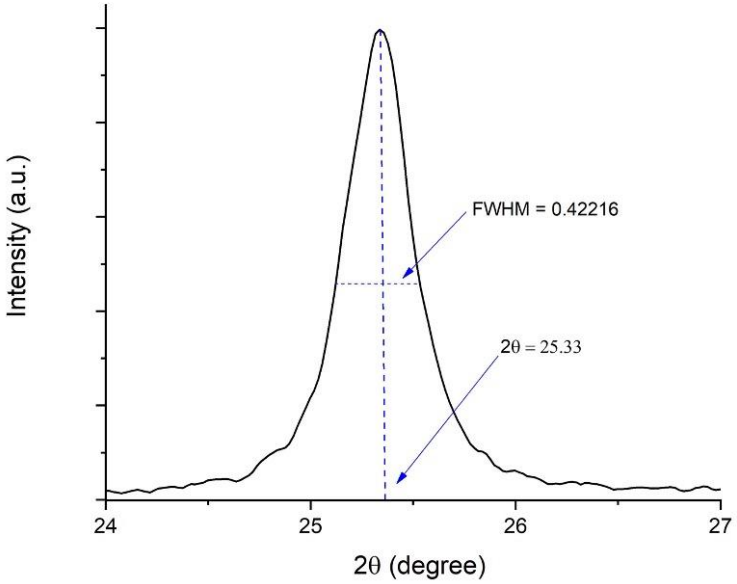

Figure 66: The half-height width of P25 at 25.33° as an anatase phase

Crystallize size of anatase TiO_2: The half-height width = 0.42216°

$$= 0.42216 \times \frac{2\pi}{360}$$

= 0.007364 radian

The peak width: $\beta = \sqrt{0.007364^2 - 0.003836^2}$

= 0.006286 radian

2θ = 25.33°

θ = 12.66°

λ = 1.5418 Å

The crystallite sizes: $D = \frac{K\lambda}{\beta\cos\theta}$

$$= \frac{0.9 \times 1.5418}{0.006286 \times \cos(12.66)}$$

= 221.84 Å

= 22.18 nm.

Calculation %Anatase = $\frac{\mathbf{0.79\ x\ I_A}}{\mathbf{I_R + (0.79\ x\ I_A)}}$ x 100 and

%Rutile = $\frac{\mathbf{I_R}}{\mathbf{I_R + (0.79\ x\ I_A)}}$ x 100

When I_A = The intensity of main anatase peak height at $2\theta = 25.33^{\circ}$

I_R = The intensity of main anatase peak height at $2\theta = 27.42^{\circ}$

So, %Anatase = $\frac{\mathbf{0.79\ x\ 499.05}}{\mathbf{93.73 + (0.79\ x\ 99.05)}}$ x 100 = 80.79%

%Rutile= $\frac{\mathbf{93.73}}{\mathbf{93.73 + (0.79\ x\ 499.05)}}$ x 100 = 19.21%

APPENDIX C

CALCULATION OF THE ENERGY BAND GAP (Eg)

Determination of electronic gap energy of semiconductor by using cut-off wavelength from spectrum using the following equation: $E_g = \frac{hc}{\lambda}$

when E_g = Energy band gap (eV)

λ = Wavelength (nm)

h = Planck's constant (4.135×10^{-15} eV.s)

c = Speed of light (3×10^{8} m/s)

For example:

Calculation for photocatalyst absorbed UV irradiation at 350 nm.

Energy band gap (E_g) = $\frac{(4.135 \times 10^{-15}\ \text{eV}\bullet\text{s}) \times (3 \times 10^{8} \frac{\text{m}}{\text{s}})}{350\ \text{nm}}$ = 3.54 eV.

Determination of energy band gap by Kubelka-Munk transform reflectance spectra with $\left[\frac{F(R_\infty)hc}{\lambda}\right]^2$ versus $\frac{hc}{\lambda}$ graph

Kubelka-Munk function is $F(R_\infty) = \frac{(1-R_\infty)^2}{2R_\infty}$

when Transform absorbent unit into reflectance $R_\infty = 10^{-A}$

R_∞ = Reflectance unit λ = Wavelength (nm)

A = absorbent unit h = Plank constant (4.135×10^{-15} eV●s)

c = Speed of light (3×10^{8} m/s)

REFERENCES

มหาวิทยาลัยศิลปากร

VITA

NAME	Chamchuri Bumrungsinmon
DATE OF BIRTH	11 November 1996
PLACE OF BIRTH	King Chulalongkorn Memorial Hospital
INSTITUTIONS ATTENDED	Department of Chemical Engineering
HOME ADDRESS	2/7 moo.3 Sampran District, Nakornpathom Province 73110
PUBLICATION	-
AWARD RECEIVED	-

1. Thamaraiselvi, K. and T. Sivakumar, *Photocatalytic reduction of carbon dioxide by using bare and copper oxide impregnated nano titania catalysts.* Journal of nanoscience and nanotechnology, 2017. **17**(1): p. 313-322.
2. Tahir, B., M. Tahir, and N.S. Amin, *Gold–indium modified TiO2 nanocatalysts for photocatalytic CO2 reduction with H2 as reductant in a monolith photoreactor.* Applied Surface Science, 2015. **338**: p. 1-14.
3. Meng, X., et al., *Photocatalytic CO 2 conversion over alkali modified TiO 2 without loading noble metal cocatalyst.* Chemical Communications, 2014. **50**(78): p. 11517-11519.
4. Peng, F., et al., *Preparation of nitrogen-doped titanium dioxide with visible-light photocatalytic activity using a facile hydrothermal method.* journal of Physics and Chemistry of Solids, 2008. **69**(7): p. 1657-1664.
5. Krejčíková, S., et al., *Preparation and characterization of Ag-doped crystalline titania for photocatalysis applications.* Applied Catalysis B: Environmental, 2012. **111**: p. 119-125.
6. Li, Y., et al., *Synthesis and characterization of Cu2O/TiO2 photocatalysts for H2 evolution from aqueous solution with different scavengers.* Applied Surface Science, 2015. **324**: p. 736-744.
7. Wang, S., et al., *The relationship between economic growth, energy consumption, and CO2 emissions: Empirical evidence from China.* Science of the Total Environment, 2016. **542**: p. 360-371.
8. Flórez-Orrego, D., J.A. Silva, and S. de Oliveira Jr, *Renewable and non-renewable exergy cost and specific CO2 emission of electricity generation: The Brazilian case.* Energy conversion and management, 2014. **85**: p. 619-629.
9. Bajorowicz, B., et al., *Application of metal oxide-based photocatalysis.* 2018.
10. Zhou, H., et al., *Biomimetic polymeric semiconductor based hybrid nanosystems for artificial photosynthesis towards solar fuels generation via CO2 reduction.* Nano Energy, 2016. **25**: p. 128-135.
11. Tan, L.-L., et al., *Visible-light-activated oxygen-rich TiO2 as next generation photocatalyst: Importance of annealing temperature on the photoactivity*

toward reduction of carbon dioxide. Chemical Engineering Journal, 2016. **283**: p. 1254-1263.

12. Baldoví, H.G., et al., *Understanding the origin of the photocatalytic CO2 reduction by Au-and Cu-loaded TiO2: A microsecond transient absorption spectroscopy study.* The Journal of Physical Chemistry C, 2015. **119**(12): p. 6819-6827.
13. Qamar, S., et al., *Ultrathin TiO2 flakes optimizing solar light driven CO2 reduction.* Nano Energy, 2016. **26**: p. 692-698.
14. Kumar, N., et al., *Polypyrrole-Promoted rGO–MoS2 Nanocomposites for Enhanced Photocatalytic Conversion of CO2 and H2O to CO, CH4, and H2 Products.* ACS Applied Energy Materials, 2020. **3**(10): p. 9897-9909.
15. Sharma, A. and B.-K. Lee, *Photocatalytic reduction of carbon dioxide to methanol using nickel-loaded TiO2 supported on activated carbon fiber.* Catalysis Today, 2017. **298**: p. 158-167.
16. Li, X., et al., *Cocatalysts for selective photoreduction of CO2 into solar fuels.* Chemical reviews, 2019. **119**(6): p. 3962-4179.
17. Adachi, K., K. Ohta, and T. Mizuno, *Photocatalytic reduction of carbon dioxide to hydrocarbon using copper-loaded titanium dioxide.* Solar energy, 1994. **53**(2): p. 187-190.
18. Tjandra, A.D. and J. Huang, *Photocatalytic carbon dioxide reduction by photocatalyst innovation.* Chinese Chemical Letters, 2018. **29**(6): p. 734-746.
19. Varghese, O.K., et al., *High-rate solar photocatalytic conversion of CO2 and water vapor to hydrocarbon fuels.* Nano letters, 2009. **9**(2): p. 731-737.
20. Laursen, S. and S. Poudyal, *Photo-and Electro-Catalysis: CO2 Mitigation Technologies*, in *Novel Materials for Carbon Dioxide Mitigation Technology*. 2015, Elsevier. p. 233-268.
21. Shehzad, N., et al., *A critical review on TiO2 based photocatalytic CO2 reduction system: Strategies to improve efficiency.* Journal of CO2 Utilization, 2018. **26**: p. 98-122.
22. Liu, B.-J., T. Torimoto, and H. Yoneyama, *Photocatalytic reduction of carbon dioxide in the presence of nitrate using TiO2 nanocrystal photocatalyst*

embedded in SiO2 matrices. Journal of Photochemistry and Photobiology A: Chemistry, 1998. **115**(3): p. 227-230.

23. Kohno, Y., et al., *Photo-enhanced reduction of carbon dioxide with hydrogen over Rh/TiO2.* Journal of Photochemistry and photobiology A: Chemistry, 1999. **126**(1-3): p. 117-123.
24. Dey, G.R., A. Belapurkar, and K. Kishore, *Photo-catalytic reduction of carbon dioxide to methane using TiO2 as suspension in water.* Journal of Photochemistry and Photobiology A: chemistry, 2004. **163**(3): p. 503-508.
25. Nasution, H.W., et al., *Photocatalytic reduction of CO2 on copper-doped Titania catalysts prepared by improved-impregnation method.* Catalysis Communications, 2005. **6**(5): p. 313-319.
26. Sobana, N., M. Muruganadham, and M. Swaminathan, *Nano-Ag particles doped TiO2 for efficient photodegradation of direct azo dyes.* Journal of Molecular Catalysis A: Chemical, 2006. **258**(1-2): p. 124-132.
27. Chang, C.-C., et al., *Photocatalytic properties of nanocrystalline TiO2 thin film with Ag additions.* Thin Solid Films, 2006. **494**(1-2): p. 274-278.
28. Kim, S.-J., et al., *Photocatalytic properties of rutile TiO2 acicular particles in aqueous 4-chlorophenol solution.* Journal of materials research, 2003. **18**(3): p. 729-732.
29. Li, X.D., et al. *Synthesis, characterization and photocatalytic activity of Nb-doped TiO2 nanoparticles*. in *Advanced Materials Research*. 2012. Trans Tech Publ.
30. Herrmann, J.-M., et al., *Characterization and photocatalytic activity in aqueous medium of TiO2 and Ag-TiO2 coatings on quartz.* Applied Catalysis B: Environmental, 1997. **13**(3-4): p. 219-228.
31. Yu, J., et al., *Fabrication and characterization of Ag–TiO2 multiphase nanocomposite thin films with enhanced photocatalytic activity.* Applied Catalysis B: Environmental, 2005. **60**(3-4): p. 211-221.
32. Wang, Q., et al., *Photocatalytic properties of porous C-doped TiO 2 and Ag/C-doped TiO 2 nanomaterials by eggshell membrane templating.* Journal of Nanoparticle Research, 2009. **11**(2): p. 375-384.

33. Kočí, K., et al., *Effect of silver doping on the TiO2 for photocatalytic reduction of CO2.* Applied Catalysis B: Environmental, 2010. **96**(3-4): p. 239-244.
34. Yuan, L. and Y.-J. Xu, *Photocatalytic conversion of CO2 into value-added and renewable fuels.* Applied Surface Science, 2015. **342**: p. 154-167.
35. Zhao, C., et al., *Ultrasonic spray pyrolysis synthesis of Ag/TiO2 nanocomposite photocatalysts for simultaneous H2 production and CO2 reduction.* International Journal of Hydrogen Energy, 2012. **37**(13): p. 9967-9976.
36. Yu, B., et al., *Photocatalytic reduction of CO2 over Ag/TiO2 nanocomposites prepared with a simple and rapid silver mirror method.* Nanoscale, 2016. **8**(23): p. 11870-11874.
37. Mekasuwandumrong, O., et al., *Influence of flame conditions on the dispersion of Pd on the flame spray-derived Pd/TiO2 nanoparticles.* Powder technology, 2011. **210**(3): p. 328-331.
38. Jang, H.D., et al., *Synthesis and characterization of indium–tin oxide (ITO) nanoparticles.* Current Applied Physics, 2006. **6**(6): p. 1044-1047.
39. Nokjan, S., *Impact of Si, Fe, Cu addition on the physiochemical and photocatalytic properties of FSP-made TiO2*. 2014, มหาวิทยาลัย ศิลปากร.
40. Gunawan, C., et al., *Reversible antimicrobial photoswitching in nanosilver.* Small, 2009. **5**(3): p. 341-344.
41. Teoh, W.Y., *A perspective on the flame spray synthesis of photocatalyst nanoparticles.* Materials, 2013. **6**(8): p. 3194-3212.
42. Unwiset, P., et al., *Effect of Cu addition on TiO2 surface properties and photocatalytic performance: X-ray Absorption Spectroscopy analysis.* Journal of Physics and Chemistry of Solids, 2018. **120**: p. 231-240.
43. Karhunen, T., et al., *Transition metal-doped lithium titanium oxide nanoparticles made using flame spray pyrolysis.* ISRN Nanotechnology, 2011. **2011**.
44. Hoffmann, M.R., et al., *Environmental applications of semiconductor photocatalysis.* Chemical reviews, 1995. **95**(1): p. 69-96.

45. Liu, Y., et al., *Degradation of phenol in industrial wastewater over the F–Fe/TiO2 photocatalysts under visible light illumination.* Chinese Journal of Chemical Engineering, 2016. **24**(12): p. 1712-1718.

46. Landmann, M., E. Rauls, and W. Schmidt, *The electronic structure and optical response of rutile, anatase and brookite TiO2.* Journal of physics: condensed matter, 2012. **24**(19): p. 195503.

47. Kudo, A. and Y. Miseki, *Heterogeneous photocatalyst materials for water splitting.* Chemical Society Reviews, 2009. **38**(1): p. 253-278.

48. Siddiqui, H., *Modification of Physical and Chemical Properties of Titanium Dioxide (TiO 2) by Ion Implantation for Dye Sensitized Solar Cells*, in *Ion Beam Techniques and Applications*. 2019, IntechOpen.

49. Lee, T.C., M.I. Idris, and H.Z. Abdullah. *Effect of UV Light Treatment Condition on Apatite Formation of Anodised Titanium*. in *Advanced Materials Research*. 2015. Trans Tech Publ.

50. Sanzone, G., et al., *Ag/TiO2 nanocomposite for visible light-driven photocatalysis.* Superlattices and Microstructures, 2018. **123**: p. 394-402.

51. Yang, Y., L. Kang, and H. Li, *Enhancement of photocatalytic hydrogen production of BiFeO3 by Gd3+ doping.* Ceramics International, 2019. **45**(6): p. 8017-8022.

52. Mekasuwandumrong, O., et al., *Photocatalytic Liquid-Phase Selective Hydrogenation of 3-Nitrostyrene to 3-vinylaniline of Various Treated-TiO2 Without Use of Reducing Gas.* Catalysts, 2019. **9**(4): p. 329.

53. Freitas, I.C., R.L. Manfro, and M.M. Souza, *Hydrogenolysis of glycerol to propylene glycol in continuous system without hydrogen addition over Cu-Ni catalysts.* Applied Catalysis B: Environmental, 2018. **220**: p. 31-41.

54. Chen, Y., et al., *Identification of carbon sensitization for the visible-light photocatalytic titanium oxide.* Journal of Vacuum Science & Technology A: Vacuum, Surfaces, and Films, 2010. **28**(4): p. 779-782.

55. Magnone, E., et al., *Testing and substantial improvement of TiO2/UV photocatalysts in the degradation of Methylene Blue.* Ceramics international, 2019. **45**(3): p. 3359-3367.

56. Yu, W., et al., *Enhanced visible light photocatalytic degradation of methylene blue by F-doped TiO2.* Applied Surface Science, 2014. **319**: p. 107-112.

57. Bakar, S.A. and C. Ribeiro, *A comparative run for visible-light-driven photocatalytic activity of anionic and cationic S-doped TiO2 photocatalysts: A case study of possible sulfur doping through chemical protocol.* Journal of Molecular Catalysis A: Chemical, 2016. **421**: p. 1-15.

58. Wu, Y.-C. and L.-S. Ju, *Annealing-free synthesis of CN co-doped TiO2 hierarchical spheres by using amine agents via microwave-assisted solvothermal method and their photocatalytic activities.* Journal of alloys and compounds, 2014. **604**: p. 164-170.

59. Kim, S., S.-J. Hwang, and W. Choi, *Visible light active platinum-ion-doped TiO2 photocatalyst.* The Journal of Physical Chemistry B, 2005. **109**(51): p. 24260-24267.

60. Vijayan, B.K., et al., *The effects of Pt doping on the structure and visible light photoactivity of titania nanotubes.* The Journal of Physical Chemistry C, 2010. **114**(49): p. 21262-21269.

61. Kočí, K., et al., *Wavelength effect on photocatalytic reduction of CO2 by Ag/TiO2 catalyst.* Chin J Catal, 2011. **32**(5): p. 812-815.

62. Vaithiyanathan, R. and T. Sivakumar, *Studies on photocatalytic activity of the synthesised TiO2 and Ag/TiO2 photocatalysts under UV and sunlight irradiations.* Water Science and Technology, 2011. **63**(3): p. 377-384.

63. Kominami, H., et al., *Copper-Modified Titanium Dioxide: A Simple Photocatalyst for the Chemoselective and Diastereoselective Hydrogenation of Alkynes to Alkenes under Additive-Free Conditions.* ChemCatChem, 2016. **8**(12): p. 2019-2022.

64. Li, J., J. Xu, and J. Huang, *Nanofibrous vanadium-doped rutile titania derived from cellulose substance by flame synthesis.* CrystEngComm, 2014. **16**(3): p. 375-384.

65. Kuvarega, A.T., R.W. Krause, and B.B. Mamba, *Nitrogen/palladium-codoped TiO2 for efficient visible light photocatalytic dye degradation.* The Journal of Physical Chemistry C, 2011. **115**(45): p. 22110-22120.

66. Wu, J.C., *Photocatalytic reduction of greenhouse gas CO 2 to fuel.* Catalysis surveys from Asia, 2009. **13**(1): p. 30-40.

67. Tan, S.S., L. Zou, and E. Hu, *Photocatalytic reduction of carbon dioxide into gaseous hydrocarbon using TiO2 pellets.* Catalysis Today, 2006. **115**(1-4): p. 269-273.

68. Zhang, Q.-H., et al., *Photocatalytic reduction of CO2 with H2O on Pt-loaded TiO2 catalyst.* Catalysis Today, 2009. **148**(3-4): p. 335-340.

69. Liu, E., et al., *Photocatalytic reduction of CO 2 into methanol over Ag/TiO 2 nanocomposites enhanced by surface plasmon resonance.* Plasmonics, 2014. **9**(1): p. 61-70.

70. Ghaly, M.Y., et al., *Treatment of highly polluted paper mill wastewater by solar photocatalytic oxidation with synthesized nano TiO2.* Chemical Engineering Journal, 2011. **168**(1): p. 446-454.

71. Ba-Abbad, M.M., et al., *Synthesis and catalytic activity of TiO2 nanoparticles for photochemical oxidation of concentrated chlorophenols under direct solar radiation.* Int. J. Electrochem. Sci, 2012. **7**(6): p. 4871-4888.

72. Wang, W.-K., et al., *Self-induced synthesis of phase-junction TiO 2 with a tailored rutile to anatase ratio below phase transition temperature.* Scientific reports, 2016. **6**: p. 20491.

73. Heidarpour, F., et al., *NANO SILVER-COATED POLYPROPYLENE WATER FILTER: I. MANUFACTURE BY ELECTRON BEAM GUN USING A MODIFIED BALZERS 760 MACHINE.* Digest Journal of Nanomaterials & Biostructures (DJNB), 2010. **5**(3).

74. Temgire, M. and S. Joshi, *Optical and structural studies of silver nanoparticles.* Radiation Physics and Chemistry, 2004. **71**(5): p. 1039-1044.

75. Khan, H. and D. Berk, *Effect of a chelating agent on the physicochemical properties of TiO 2: characterization and photocatalytic activity.* Catalysis letters, 2014. **144**(5): p. 890-904.

76. Verma, P. and S.K. Samanta, *Degradation kinetics of pollutants present in a simulated wastewater matrix using UV/TiO 2 photocatalysis and its microbiological toxicity assessment.* Research on Chemical Intermediates, 2017. **43**(11): p. 6317-6341.

77. Jiang, Y., et al., *Natural assembly of a ternary Ag–SnS–TiO 2 photocatalyst and its photocatalytic performance under simulated sunlight.* RSC advances, 2018. **8**(24): p. 13408-13416.

78. Anpo, M., et al., *Photocatalytic reduction of CO2 with H2O on various titanium oxide catalysts.* Journal of Electroanalytical Chemistry, 1995. **396**(1-2): p. 21-26.

79. Zieliński, A., et al., *Silver-doped TiO2 prepared by microemulsion method: Surface properties, bio-and photoactivity.* Separation and Purification Technology, 2010. **72**(3): p. 309-318.

80. Liang, Y., et al., *Silver nanoparticles supported on TiO2 nanotubes as active catalysts for ethanol oxidation.* Journal of Catalysis, 2011. **278**(2): p. 276-287.